Accepted by The Astrophysical Journal
Preprint typeset using LaTeX style emulateapj v. 10/10/03

THE DISCOVERY OF CEPHEIDS AND A DISTANCE TO NGC 5128[1]

Laura Ferrarese[2], Jeremy R. Mould[3], Peter B. Stetson[2], John L. Tonry[4], John P. Blakeslee[5], & Edward A. Ajhar[6]

Accepted by The Astrophysical Journal

ABSTRACT

We discuss a new distance to NGC 5128 (Centaurus A) based on Cepheid variables observed with the *Hubble Space Telescope*. Twelve F555W (V) and six F814W (I) epochs of cosmic-ray-split *Wide Field Planetary Camera 2* observations were obtained. A total of 56 *bona-fide* Cepheids were discovered, with periods ranging from 5 to $\sim$ 50 days; five of these are likely Population II Cepheids of the W Virginis class, associated with the bulge or halo of NGC 5128. Based on the period and V and $I-$band luminosities of a sub-sample of 42 classical (Pop I) Cepheids, and adopting a Large Magellanic Cloud distance modulus and extinction of 18.50 ± 0.10 mag and E$(B-V)$=0.10 mag, respectively, the true reddening-corrected distance modulus to NGC 5128 is $\mu_\circ = 27.67 \pm 0.12$ (random) ± 0.16 (systematic) mag, corresponding to a distance of 3.42 ± 0.18 (random) $\pm$ 0.25 (systematic) Mpc. The random uncertainty in the distance is dominated by the error on the assumed value for the ratio of total to selective absorption, R_V, in NGC 5128, and by the possible metallicity dependence of the Cepheid Period-Luminosity relation at V and I. This represent the first determination of a Cepheid distance to an early-type galaxy.

Subject headings: Cepheids — distance scale — galaxies: distances and redshifts — galaxies: individual (NGC 5128)

1. INTRODUCTION

The HST Key Project on the Extragalactic Distance Scale (Mould et al. 2000a; Freedman et al. 2001) and the HST project on the "Calibration of Nearby Type Ia Supernovae" (Sandage et al. 1992) have greatly improved our knowledge of the Hubble Constant by providing a solid zero point for distance indicators applicable to Population I (Pop I) stellar systems, in particular the Tully- Fisher (TF) relation (Sakai et al. 2000) and Type Ia Supernovae (SNIa; Saha et al. 2001; Gibson et al. 2000). This goal was achieved by measuring accurate Cepheid distances to over two dozen nearby spiral galaxies, in which Cepheid, TF and/or SNIa distances could be compared directly. The calibration of distance estimators applicable to early-type galaxies cannot benefit from such direct comparison, leading to considerable disagreement in the Population II (Pop II) distance scale (Ferrarese et al. 2000; Blakeslee et al. 2002; Ciardullo et al. 2002). Resolving such discrepancies is a must, not only as a means of checking for systematic errors in the Pop I distance scale ladder, but also for the practical reason that early-type galaxies are found in all types of environments, that they are more abundant than spirals in rich clusters, and that they enjoy a privileged position in a cluster's gravitational center.

Pop II distance indicators include several classes of variable stars (most notably RR-Lyrae, e.g. Dolphin et al. 2001 and references therein, and Mira Variables, e.g. Feast et al. 1989), the Tip of the Red Giant Branch (TRGB; e.g. Mould & Kristian 1986), the red clump (Paczynski & Stanek 1998; Udalski 2000), the Surface Brightness Fluctuation method (SBF; Tonry & Schneider 1988), the Planetary Nebula Luminosity Function (PNLF; Jacoby et al. 1999), the Globular Cluster Luminosity Function (GCLF; e.g. Richtler 2003), the Globular Cluster Sizes (GCS, Jordán et al. 2005), and the Fundamental Plane (FP; Dressler et al. 1987; Djorgovski & Davis 1987). PNLF and TRGB can be used with equal success across the entire Hubble sequence and provide, at least in local galaxies, a direct link between the Pop II and the Pop I (Cepheids in particular) distance scales. Although all methods can be used to study local deviations from the Hubble flow (see Méndez et al. 2002 for an application using the TRGB), SBF and the FP have the additional advantage of being the only estimators, besides TF and SNIa, to extend far enough into the unperturbed Hubble flow to allow a direct measurement of the Hubble constant. SBF in particular benefits from an intrinsic scatter which only SNIa can rival (Tonry et al. 2001), making it an order of magnitude less susceptible than TF to Malmquist biases and systematic error.

As a step in securing a Cepheid-based calibration of Pop II distance indicators, we present in this paper the first determination of a Cepheid distance to an early-type galaxy. Our target is the giant elliptical NGC 5128. The

[1] Based on observations with the NASA/ESA *Hubble Space Telescope* obtained at the Space Telescope Science Institute, which is operated by the association of Universities for Research in Astronomy, Inc., under NASA contract NAS 5-26555.

[2] Herzberg Institute of Astrophysics, National Research Council of Canada, 5071 West Saanich Road, Victoria, BC, V8X 4M6, Canada; laura.ferrarese@nrc-cnrc.gc.ca, peter.stetson@nrc-cnrc.gc.ca
[3] National Optical Astronomy Observatory, P.O. Box 26732, Tucson, AZ 85726, USA; jrm@noao.edu
[4] Institute for Astronomy, University of Hawaii, 2680 Woodlawn Drive, Honolulu, HI 96822, USA; jt@ifa.hawaii.edu
[5] Department of Physics and Astronomy, PO Box 642814, Washington State University, Pullman, WA 99164, USA; jblakes@wsu.edu
[6] Department of Natural Sciences, Mathematics, and Computer Science, St. Thomas University, 16401 NW 37th Avenue, Miami Gardens, FL 33054, USA; ajhar@stu.edu

galaxy is the dominant member of the Centaurus group, a powerful radio galaxy (Centaurus A), the host of the very well sampled (but highly reddened) SNIa SN1986G (Phillips et al. 1987), and an archetypal merger (Malin, Quinn & Graham 1983). Its Pop I component, including the Cepheids, is supported by the reservoir of gas (Oosterloo et al. 2002) deposited in the merger; star formation is triggered partly by the merger and partly by interaction between the gas cloud and the radio jet (Mould et al. 2000b). Distances to NGC 5128 have been measured using the TRGB in the halo (Soria et al. 1996; Harris et al. 2002; Rejkuba et al. 2005), SBF (Tonry et al. 2001), PNLF (Hui et al. 1995), and GCLF (Harris et al. 1988). In future contributions, we will discuss a Cepheid distance to NGC 4647, a spiral galaxy interacting with the giant elliptical NGC 4649, strategically located in the Virgo cluster core. A revision of the zero points for Pop II distance indicators, and SBF in particular, will also be presented.

The paper is organized as follows. In §2 we present the multi-epoch *Hubble Space Telescope* (HST) *Wide Field Planetary Camera 2* (WFPC2) observations on which our distance determination is based. The photometric analysis is discussed in §3, while the identification of Cepheids and their derived properties are discussed in §4. The derived distance to NGC 5128 is presented in §5. The result is discussed and contrasted with previous distance determinations for NGC 5128 and the Centaurus group in §6, where conclusions can also be found.

2. OBSERVATIONS AND INITIAL DATA REDUCTION

NGC 5128 was observed between 2001 July 8 and 2001 August 20 as part of program GO-9043. The 44-day length of the observing window was imposed by the need to observe the field at a single orientation, i.e., without changing the roll angle of the telescope. Within this window, WFPC2 F555W (similar to Johnson V) and F814W ($\sim$ Kron-Cousins I) images were taken at 12 and six epochs respectively, spaced in such a way to optimize the discovery of variable stars with period between ~ 10 and 50 days, as described in Freedman et al. (1994). Each image was split in a pair of consecutive exposures, referred to as a "cosmic ray-split pair", of duration between 1100 and 1400 s. Details of the observing procedure, including the calendar and Heliocentric Julian Date (HJD) of the observations, the HST archive rootnames, the filter employed, and exposure times are listed in Table 1.

The WFPC2 field of view (FOV) is divided between three *Wide Field Cameras* (WFC), each with pixel scale of $0''.1$, and one *Planetary Camera* (PC), with pixel scale of $0''.046$. The FOV of each WFC is $80''\times80''$, while the FOV of the PC is $36''.8\times36''.8$. Figure 1 shows the position of the WFPC2 FOV superimposed to a ground-based image of NGC 5128. The region targeted purposely avoided the high background associated with the galaxy core, and included the western edge of the equatorial dust lane, where the abundance of recent star formation should prove conducive to the detection of Cepheids. To minimize the impact of dead pixels and other CCD imperfections, at each epoch the telescope pointing was offset slightly (up to $2''.6$ relative to the first epoch) following a spiral hexagonal pattern. All observations were obtained with the telescope pointing in fine lock, giving a nominal pointing stability of 5 mas (RMS) or better over 60-second intervals.

Basic data reduction (bias removal, dark subtraction and flat fielding) was performed by the IRAF task CALWP2 when downloading the images from the STScI data archive, selecting the "On the Fly Reprocessing" option. Details of the calibration procedures executed by CALWP2 can be found in the WFPC2 Data Handbook (Heyer et al. 2005).

3. PHOTOMETRIC ANALYSIS

The photometric reduction was performed independently using a variant of DoPHOT (Schechter, Mateo & Saha 1993; Saha et al. 1994) and DAOPHOT II/ALLFRAME (Stetson 1994). A detailed description of the photometric reduction process can be found in Ferrarese et al. (1996) and Stetson et al. (1998). In what follows, we only provide a brief summary of the key steps.

3.1. *DoPHOT Procedure*

Unlike ALLFRAME, DoPHOT works most effectively on images which have been cleaned of cosmic ray (CR) hits. CR-split pairs were therefore combined using a sigma detection algorithm which takes into account the problems of Point Spread Function (PSF) undersampling (Saha et al. 1996). The DoPHOT reduction of the resulting 12 F555W and six F814W images was performed using as first guess a parametric representation of the PSF which best represents point sources in the frames. To aid source detection, the photometric reduction of each epoch adopts, as a starting point, an input star-list generated by running DoPHOT on deep, CR-free F555W and F814W images, respectively created by combining all 24 F555W and 12 F814W frames listed in Table 1. In combining the frames, single images are first brought into alignment with the first epoch frames, using shifts calculated by matching positions for a list of objects in common; rotations between frames were found to be negligible in all cases. To insure photometric stability, in aligning the images sub-pixel interpolation was not performed and images were not corrected for geometric distortion. Although this unavoidably leads to a degradation in the PSF of the deep frames relative to that of the single exposures, this has no detrimental effects on the photometry.

DoPHOT magnitudes are defined as $m_{Do} = -2.5\log(\mathrm{DN}/t)+30.0$, where DN is the number of counts within an aperture of radius equal to 5 pixels, and t is the exposure time. The raw output from DoPHOT is converted to DoPHOT magnitudes by applying an aperture correction, calculated by performing aperture photometry on bright isolated stars. Telescope jitter or focus changes between subsequent epochs can result in a slight time dependence of the aperture corrections, however, rather than deriving independent aperture corrections for each epoch/filter, we instead derived aperture corrections from the deep images (using between 35 and 160 stars depending on the filter/chip), applied them to each epochs' photometry, matched the deep frame photometry to that of the first epoch (both of which have been aperture corrected), and finally matched each epoch's aperture-corrected photometry to the aperture-corrected

deep photometry. With this procedure, the first epoch is used to tie the photometry, the aperture corrections are derived from the high signal-to-noise deep images, and small changes in aperture corrections are accounted for by (effectively) matching the photometry of several thousand stars in each epoch to that of the first. The deep frames are not used directly to tie the photometry because of possible complications introduced by the degradation in the PSF as a result of the procedure used to combine the single exposures. Variations in aperture corrections between epochs are found to be 0.03 mag or less.

3.2. *ALLFRAME*

ALLFRAME is run directly on the single exposures, without combining CR-split pairs or rejecting cosmic rays. An input star list to ALLFRAME was generated from median-averaged cosmic-ray-free F555W and F814W deep frames. Iterative application of DAOPHOT and ALLSTAR led to a single final master star list, including stars detected in either (or both) filters. This star list was input to ALLFRAME, and used to extract profile-fitting stellar photometry from the 36 individual frames. The adopted PSFs were derived from public domain HST WFPC2 observations of the globular clusters Pal 4 and NGC 2419.

Aperture photometry was performed on a set of bright isolated stars. The program DAOGROW was then employed to generate growth curves out to $0''.5$, allowing an aperture correction to be derived for each chip and filter, using the approach of Holtzman et al. (1995). As seen for the DoPHOT photometry, variations in aperture corrections for the same filter/chip and different epochs are found to be, on average, 0.03 mag or less.

3.3. *Absolute Photometric Calibration*

The continuing degradation in the WFPC2 performance demands a frequent updating of the coefficients needed to convert DoPHOT and ALLFRAME magnitudes to standard-system magnitudes, m_{F555W} and m_{F814W}, and ultimately, through the adoption of a color term, to Johnson V and Kron-Cousin I. As part of this project, we obtained F555W and F814W WFPC2 single-epoch images of the Draco dwarf spheroidal, and three globular clusters, NGC 5262, NGC 6341 and NGC 2419. Comparison of ground-based and HST ALLFRAME photometry for secondary standard stars in these fields has led to the updated ALLFRAME photometric calibration equations listed in Table 2. The transformations assume a color correction as in Holtzman et al. (1995), so that only the zero points are derived when matching the HST to the ground-based photometry; a full description of the procedure will be provided in an upcoming paper (Stetson, in preparation). These transformations were derived using 40 s F555W and F814W exposures, and are therefore equivalent to the "short-exposure zero points" presented in Hill et al. (1998). Comparing the Hill et al. to the new coefficients implies a 10 to 15% degradation in the WFPC2 performance (slightly worse in F555W than in F814W) between May 1994 (when the fields analyzed by Hill et al. were observed) and July 2001. Comparing the new coefficients to those presented by Dolphin (2000, for a "cold" operating temperature and gain = 7), which were derived from data taken between January 1994 and May 2000, implies a 5 to 10% degradation in the WFPC2 performance (again slightly worse in F555W than in F814W).

There is some debate in the literature as to whether the photometric zero points differ depending on whether short ($\lesssim$ 60 s) or long exposure ($\gtrsim$1300 s) observations are used in their derivation. Hill et al., as well as previous investigations, find that zero points obtained from the long exposure observations are systematically fainter, on average by 0.05 mag, with no significant chip/filter dependence, while Dolphin (2000) find no evidence of such effect. In addition to the 40 s exposures mentioned above, exposures between 230 and 300 s were obtained for all standard fields (Draco, NGC 5262, NGC 6341 and NGC 2419) at the same time as the NGC 5128 frames; comparing these longer exposures (analyzed with ALLFRAME as described in the previous paragraph) to the 40 s exposures yields zero points which are on average 0.025 to 0.030 mag fainter than those reported in Table 2 (again with no significant dependence on chip/filter), in the same sense noted by Hill et al., i.e., the detector quantum efficiency appears to be reduced in the shorter exposure. In light of this, we assume a 0.05 mag difference, in both V and I, between the zero points listed in Table 2 and those applicable to the longer NGC 5128 exposures. *In the rest of this paper, all tables and Figures use the short exposure zero points given in Table 2, however, we will add 0.05 mag to the final distance modulus to account for the fact that the NGC 5128 frames used longer exposures time than the standard fields from which the photometric calibration is derived.* We will include the uncertainty in the photometric zero points in the discussion of the error budget in §5.3.

Analogous transformation equations applicable to the DoPHOT photometry were obtained by comparing the DoPHOT and ALLFRAME photometry for a set of bright, isolated secondary standard stars (listed in the Appendix) in the NGC 5128 field. Figure 2 shows a chip-by-chip comparison of the $V-$ and $I-$band ALLFRAME and DoPHOT photometry for these secondary standards, the former adopting the transformations listed in Table 2, and the latter using the short exposure zero points from Hill et al. (1998). Mean differences between the DoPHOT and ALLFRAME photometry are listed in Table 3 for each chip/filter combination. The slightly larger offsets noted for the PC (and more so in I than in V) could be due to several causes, including a slight degradation in the PSF (the size of the aperture, in arcsec, used in measuring DoPHOT magnitudes is smaller in the PC than in the WF chips) between 1994 and 2001, and/or a change in the Charge-Transfer Inefficiency (CTE) which is known to affect WFPC2 data (Stetson 1998).

Bringing the DoPHOT photometry into agreement with the ALLFRAME photometry by correcting for the observed offsets leads to the DoPHOT photometric transformations listed in Table 4. Figure 3 shows the match between the DoPHOT and ALLFRAME photometry for the same secondary standard stars shown in Figure 2 once these final zero points are adopted. It is worth noticing that a small scale error appears to be present in the $I-$band comparison. Regression fits, accounting for

errors in both variables, to the data shown in Figure 3 give:

$$V_{\rm DoPHOT} - V_{\rm ALLFRAME} = -(0.0023 \pm 0.0080) - \\ - (0.006 \pm 0.012) \times (V_{\rm DoPHOT} - 22.72) \quad (1)$$

$$I_{\rm DoPHOT} - I_{\rm ALLFRAME} = -(0.0047 \pm 0.0030) - \\ - (0.0202 \pm 0.0049) \times (I_{\rm DoPHOT} - 21.43) \quad (2)$$

Scale errors of this magnitude are not uncommon when comparing DoPHOT and ALLFRAME photometry (e.g. Hill et al. 1998), and are likely to reflect the inherent limitations of PSF fitting procedures in crowded fields. In the worst case scenario, i.e. assuming that the error resides entirely with the DoPHOT photometry (which will be used in §5 to measure the distance to NGC 5128), the $I-$band 0.02 mag/mag scale error would lead to overestimate the magnitudes of the faintest Cepheids (mean $I-$band magnitude $\sim$ 23.5) by $\sim$ 0.04 mag ($I_{\rm DoPHOT}$ and $I_{\rm ALLFRAME}$ agree at the mean magnitudes of the brightest Cepheids). Correcting all DoPHOT photometry according to equation (2) would increase all distances (derived using the same procedure discussed in §5) by 0.04 mag. However, given the uncertain nature of this scale error, and its limited impact compared to all other sources of error which will be discussed in §5.3, we feel justified in neglecting its effects in the remainder of this paper.

Finally, we note that the zero points listed in Tables 2 and 4 do not include a correction for CTE. The electron loss due to CTE is dependent on position within the chip, as well as on the brightness of the star and underlying sky background. The zero points used in this paper are translated to the chips' centers; therefore we expect that (uncorrected) CTE losses will add scatter (at the few hundredths of a magnitude level) in the photometry, but not produce any systematic biases in the photometry of a sample of stars distributed uniformly throughout the chip. We note that the combination of $V = 20$ mag standards and 80 second exposures with $V = 25$ mag Cepheids and 1100 second exposures leads to equal CTE corrections for both Cepheids and standards, according to the coefficients of Stetson (1998). Although we assume that this remained true for our 2001 data, we expect to test this assumption in ongoing calibration work.

4. CEPHEID IDENTIFICATION

The search for variable stars was conducted using three independent methods: 1) a variant of Stellingwerf's (1978) phase dispersion minimization routine, as described in Saha & Hoessel (1990), applied to the DoPHOT photometry; 2) the template light curve fitting algorithm TRIAL (Stetson 1996) applied to the ALLFRAME photometry; and 3) a photometry-independent image subtraction method, following Alard & Lupton (1998). The first two methods produce both a list of likely variables and an estimate of the variability period, while the third method was implemented to simply flag objects undergoing luminosity variations, with no attempt to construct light curves.

Every star that satisfies the variability criteria imposed by the previous methods was visually inspected by blinking the images against each other. This step is necessary since random errors in the photometry, uncorrected CR hits, or crowding, do occasionally result in spurious light curves which look credible based on the photometry alone. Of the 126 variables identified based on one or more of the methods above, a total of 56 were judged to be *bona-fide* Cepheid variables based on the character of the light curve, the visually-established reliability of the light variations, and some visual assurance that the star does not appear to be a blend or is found in an unusually crowded region. The remaining 70 stars are likely genuine variables, although either their photometry is considered suspect because of crowding, or their light curves do not appear Cepheid-like.

For the remainder of this paper, we will adopt the DoPHOT photometry for all variables. The periods quoted are therefore determined based on method 1) above; a comparison of these periods and the TRIAL periods best fitting the ALLFRAME light curves for the 36 *bona-fide* Cepheids in common shows excellent agreement, with a mean difference of $(-0.5 \pm 5.4)\%$.

For each variable star, we calculated both intensity-averaged magnitudes, defined as

$$m = -2.5 \log_{10} \sum_{i=1}^{n} \frac{1}{n} 10^{-0.4 \times m_i}, \quad (3)$$

and phase-weighted magnitudes (Saha and Hoessel 1990), defined as

$$m = -2.5 \log_{10} \sum_{i=1}^{n} 0.5(\phi_{i+1} - \phi_{i-1}) 10^{-0.4 \times m_i}, \quad (4)$$

where the phase ϕ varies between 0 and 1. In the above equations, n is the total number of observations, and m_i and ϕ_i are the magnitude and phase of the $i-$th observation in order of increasing phase. Phase-weighted magnitudes are more robust than intensity-averaged magnitudes for variables with non-uniform temporal sampling (Saha and Hoessel, 1990).

X and Y positions within the chip (in the coordinate frame of the first epoch), right ascension and declination, period, intensity-averaged and phase-weighted V and I magnitudes for all Cepheids are listed in Table 5, while parameters for the suspected variable stars are listed in the Appendix, where single epoch F555W and F814W magnitudes of all Cepheids are also reported. Note that for Cepheids which vary on timescales close to or longer than the 44-day contiguous observing window, often only a lower limit on the period can be placed.

The spatial distribution of the Cepheids and suspected variable stars in each chip is shown in Figure 4. Detailed finding charts are given in Figure 5 for the Cepheids, and in the Appendix for the suspected variable stars.

DoPHOT light curves for each Cepheid, phased to the appropriate period, are presented in Figure 6 – the F555W and F814W magnitudes are shown by solid and open dots, respectively. Figure 7 shows the location of

the 56 Cepheids (using phase-weighted V and I magnitudes) listed in Table 5 in a $V, V-I$ color-magnitude diagram (CMD), constructed using the DoPHOT photometry of the deep F555W and F814W frames; mean photometric errors, calculated in bins of width equal to 0.5 mag, are shown in Figure 8 as a function of magnitude and color. Note that in Figure 7, most Cepheids lie outside the instability strip, which is shown in the Figure assuming a $V-$band distance modulus of 28.85 mag and reddening $E(V-I) = 0.55$ mag (see §5). As will be discussed in §5, this is a consequence of the large and highly position dependent reddening of the NGC 5128 field.

5. THE DISTANCE TO NGC 5128

5.1. *Standard Procedure*

The DoPHOT $V-$ and $I-$band Period-Luminosity (PL) relations for NGC 5128 are shown in the upper panels of Figure 9, using phase-weighted magnitudes. Cepheids identified by a symbol with an arrow are those for which only a lower limit on the period could be placed. In the lower two panels of Figure 9, the $< V >$ and $< I >$ phase-weighted magnitudes are combined to give the Wesenheit function $W = V - (V-I) \times A(V)/E(V-I)$ (Madore 1982). By construction, W is unaffected by line-of-sight reddening, therefore the extrinsic scatter in the $W - \log P$ plane should be smaller than in either the $< I > - \log P$ or (especially) $< V > - \log P$ planes. The lower right panel of Figure 9 shows the same data plotted in the lower left panel, but Cepheids are color-coded according to the chip to which they belong.

The apparent $V-$ and $I-$band distance moduli (i.e. $\mu_{\rm V}$ and $\mu_{\rm I}$) to NGC 5128 are derived relative to those of the Large Magellanic Cloud. We adopt the LMC PL relations of Udalski et al. (1999), scaled to a true LMC distance modulus of $\mu_{\circ,LMC} = 18.50 \pm 0.10$ mag and reddening $\mathrm{E}(B-V)_{LMC} = 0.10$ mag as in Freedman et al. (2001):

$$M_V = -2.760[\pm0.03](\log P - 1.0) - 4.218[\pm0.02] \quad (\sigma_V = \pm0.16) \tag{5}$$

and

$$M_I = -2.962[\pm0.02](\log P - 1.0) - 4.904[\pm0.01] \quad (\sigma_I = \pm0.11). \tag{6}$$

Once a ratio of total to selective absorption $R_V = A(V)/E(B-V)$ and a reddening law are adopted, a reddening corrected true distance modulus μ_0 can be calculated *for each* of the NGC 5128 Cepheids. In the absence of a metallicity dependence of the Cepheid PL relation, and for a reddening law as derived by Cardelli, Clayton & Mathis (1989) with $R_V = 3.3$[7], the true distance modulus for each individual Cepheid becomes:

$$\begin{aligned}\mu_0 &= \mu_V - A(V) = \mu_I - A(I) = \\ &= \mu_V - A(V)/E(V-I)(\mu_V - \mu_I) = \\ &= 2.497\mu_I - 1.497\mu_V = \\ &= W + 3.27[\pm0.01](\log P - 1) + 5.94[\pm0.01] \\ &\quad (\sigma_0 = \pm0.08).\end{aligned} \tag{7}$$

The true distance modulus to NGC 5128 is then taken as the average of the distance moduli to the individual Cepheids. In the process, Cepheids which deviate by more than 0.48 mag (two times the width of the instability strip) from the main ridge-line of the $W - \log P$ plot are excluded from the fit. These Cepheids are shown as solid dots surrounded by larger circles in Figure 9; note that the rejection is not performed based on the V and I PL relations, for which large deviations could be due to differential reddening. In addition, Cepheids with period less than 8 days, which could be overtone pulsators (open circles in Figure 9), and Cepheids for which only a lower limit on the period could be determined, were also excluded from the fits. The procedure described above is equivalent to 1) finding the sample-mean V and I magnitudes at $\log P = 1$ by fitting V and I PL relations to the NGC 5128 data, with slopes fixed to those of equations (5) and (6); 2) subtracting them from the zero points of equations (5) and (6) respectively, to find sample-mean distance moduli μ_V and μ_I; and 3) applying the middle expression of equation (7) to derive μ_0.

Table 6 lists the distances obtained by means of the method described above. Using Cepheids from all chips, with period > 8 days and excluding outliers (case 1 in the Table), the resulting apparent distance moduli are $\mu_V = 28.85 \pm 0.10$ mag and $\mu_I = 28.30 \pm 0.06$ mag (short exposure zero points). The corresponding true distance modulus is $\mu_0 = 27.48 \pm 0.05$ mag, giving a linear distance of 3.4 ± 0.1 Mpc, where the quoted uncertainties are 1σ fitting uncertainties. These fits are shown by the solid lines in Figure 9, while the dotted lines represent 2σ deviations from the mean of the LMC relations (i.e. 0.32 mag in V, and 0.22 mag in I, equations 5 and 6).

Previous papers have noted the importance of testing the sample for incompleteness bias (e.g. Lanoix, Paturel, & Garnier 1999) by imposing a long pass filter on the period distribution. Table 6 lists distance moduli obtained by applying lower period cutoffs of 15, 20, 25 and 30 days (cases 2 to 5). In all cases, the distances agree well within the quoted uncertainties. The same is true if distances are derived independently for the four chips (cases 6 to 9). Finally, if all the suspected variable stars listed in the Appendix with period > 8 days are added to the Cepheid sample, the distance remains virtually unchanged (case 10).

Using all Cepheids with period > 8 days gives a total (foreground plus intrinsic) reddening to NGC 5128 of $E(V-I) = 0.55 \pm 0.05$ mag. The uncertainty in this estimate is not simply the quadrature sum of the uncertainties in the apparent moduli (Stetson et al. 1998): because $A(V) \propto \mu_V - \mu_I$, the intrinsic scatter in the PL relation does not propagate into the reddening uncertainty.

[7] $R_V = 3.3$ was adopted in all Key Project papers (e.g. Freedman et al. 2001), and is in agreement with the recent estimate by McCall (2004). Under these conditions, $A(\mathrm{F814W})/A(V) = 0.599$, $A(\mathrm{F555W})/A(V) = 0.999$, and $A(\mathrm{F555W})/[A(\mathrm{F555W}) - A(\mathrm{F814W})] = 2.497$

The DIRBE/IRAS dust maps of Schlegel, Finkbeiner & Davis (1998) show a foreground reddening component of $E(B-V) = 0.115$ or $E(V-I) = 0.152$ mag along the sight-line to NGC 5128, implying an average $A(V) = 1.0$ mag of internal extinction for the NGC 5128 Cepheids.

5.2. *The Effect of Reddening on the Distance to NGC 5128*

One complication in the analysis described in §5.1 is that it relies on an assumed value for R_V which, in the case discussed above, was set to 3.3 for both NGC 5128 and the LMC. For a different R_V, the coefficients in equation (7) will change, and the distance will be affected. Furthermore, as demonstrated in Ferrarese et al. (1996), if R_V differs in the LMC and NGC 5128, μ_0 becomes mildly dependent on the absolute absorption $A(V)$ to the LMC:

$$\mu_0 = \mu_V - \left[\frac{A(V)}{E(V-I)}\right]^{N5128} (\mu_V - \mu_I) + \\ + 0.582 \left[\frac{E(B-V)}{E(V-I)}\right]^{N5128} \left[\frac{R_V^{N5128}}{R_V^{LMC}} - 1\right] A(V)^{LMC} \quad (8)$$

In their study of the wavelength of maximum polarization of SN1986G, Hough et al. (1987) found $R_V = 2.4 \pm 0.13$ for the dust affected regions of NGC 5128, significantly different from the standard value of 3.3 adopted in §5.1. The generalized reddening law of Cardelli, Clayton & Mathis (1989) applied to equation (8) then yields the following expression for the true distance modulus, to be compared with equation (7):

$$\mu_0 = 2.143\mu_I - 1.143\mu_V - 0.047 \quad (9)$$

In the last two columns of Table 6, distance moduli are calculated assuming $R_V = 3.3$ for the LMC and $R_V = 2.4$ for NGC 5128. The distance modulus increases by 0.14 mag relative to the case in which $R_V = 3.3$ for both galaxies, from $\mu_0 = 27.48 \pm 0.05$ to $\mu_0 = 27.62 \pm 0.04$ for the complete sample (case 1).

The issue is explored further in Figure 10, where dereddened distance moduli are shown as a function of the value of R_V assumed for NGC 5128 (in all cases, $R_V = 3.3$ for the LMC). The upper panel of the Figure shows the standard deviation around the best-fit line in the $P-W$ plot as a function of R_V, while the lower panel shows the corresponding variation in μ_0. The scatter in the $P-W$ relation is minimized around $R_V \sim 1.8$; at this value $\mu_0 = 27.76 \pm 0.04$, corresponding to a linear distance of 3.56 ± 0.07 Mpc. We refrain from being guided by considerations of the scatter in the $P-W$ relation in choosing R_V; further insight into the nature of the reddening in NGC 5128 will require infrared photometry following Macri et al. (2001).

5.3. *Error Estimates and a Final Distance*

In view of the discussion above, and given the existence of an independent estimate of R_V in NGC 5128, we adopt as our final distance to NGC 5128 that obtained for $R_V^{NGC5128} = 2.4$ and $R_V^{LMC} = 3.3$. In what follows, however, we will take a conservative approach in quoting the uncertainty in the final distance, specifically to account for possible differences between the reddening to SN1986G and that of our Cepheid sample.

The errors listed in §5.1 and §5.2 reflect internal errors alone, arising from scatter in the NGC 5128 PL relations. A more complete assessment of the associated uncertainty, incorporating other currently identified random and systematic errors, is presented in Table 7. Uncertainties due to metallicity, LMC distance modulus (±0.10 mag, Madore & Freedman 1991; Westerlund 1996; Freedman et al. 2001), reddening and photometric calibration all contribute to the NGC 5128 distance modulus error budget. Of these, we identify as "systematic" those sources of error that affect equally all Cepheid distances derived using the same instrumental setup and calibration of the LMC PL relations as those used in this paper.

Errors related to reddening estimates in NGC 5128 contribute 0.08 mag to the (random) error budget. This is calculated following equation (8), assuming $R_V^{NGC5128} = 2.4 \pm 0.3$ and $R_V^{LMC} = 3.3$. The error on $R_V^{NGC5128}$ assumes that the difference between $R_V = 2.4$ and 3.3 represents a 3σ uncertainty on the true value of R_V. The 1σ uncertainty on A_V^{LMC} is assumed to be 0.05 mag.

The remaining random uncertainty in Table 7 which should be noted here is that due to a possible metallicity dependence of the Cepheid PL relation at V and I. Sakai et al. (2004) find a metallicity dependence of the form $d\mu_\circ/d[O/H] = -0.24 \pm 0.05$ mag/dex. This is in agreement with Groenewegen et al. (2004), although we note that Romaniello et al. (2005) find an [Fe/H] dependence of approximately the same size, but opposite sign. If the NGC 5128 Cepheids differ substantially in metal abundance from those of the LMC Cepheids which calibrate the PL relation, a significant systematic error could be present in the derived distance. Since the source of the neutral hydrogen gas for the Pop I in NGC 5128 is a galaxy like the LMC, one might expect parity in metal abundance. The H I masses of NGC 5128 and the LMC are 7.2×10^8 $M_\odot$ and 3.1×10^8 $M_\odot$ respectively (van Gorkom et al. 1990; Luks & Rohlfs 1992). On the other hand, Sutherland, Bicknell and Dopita (1994) were able to fit spectra of the jet-excited knots in Cen A with solar abundances. In these circumstances, we are unable to correct the NGC 5128 distance for the LMC/NGC 5128 metallicity difference, however we can account for it in our error estimate. Adopting [O/H]= −3.5 for the LMC Cepheids (Kennicutt et al. 1998) and assuming solar metallicity for NGC 5128, the metallicity trend of Sakai et al. (2004) leads to a $0.35 \times 0.24 = 0.08$ mag uncertainty in the distance modulus, which we include in our final error budget.

In light of the uncertainties listed in Table 7, *our final quoted Cepheid-based true distance modulus to NGC 5128 is (adding 0.05 mag to bring the photometry on the long exposure zero points, see §3.3)* $\mu_\circ = 27.67 \pm 0.12$ (random) ± 0.16 (systematic) *mag, with a reddening of* $E(V-I) = 0.55 \pm 0.05$ *(internal+foreground). The corresponding distance is* 3.42 ± 0.18 (random) ± 0.25 (systematic) *Mpc.*

6. DISCUSSION AND CONCLUSIONS

The most extensive study of the structure of the Centaurus A group has been published by Karachentsev et al. (2002). Based on HST/WFPC2 TRGB distances to 17 dwarf galaxies, the authors conclude that the group is composed of two spatially distinct substructures, with NGC 5128 and NGC 5236 (M 83) as dominant members. The mean TRGB distances to the two substructures are found to be 3.63 ± 0.07 Mpc ($\mu_0 = 27.80 \pm 0.04$ mag), and 4.57 ± 0.05 Mpc ($\mu_0 = 28.30 \pm 0.02$ mag), respectively; the latter agrees with the Cepheid distance modulus ($\mu_0 = 28.25 \pm 0.15$ mag) measured for NGC 5236 itself by Thim et al. (2003). A Cepheid distance exists for an additional member of the Cen A group, NGC 5253, host of the Type Ia SN1972E, although its value is controversial ($27.61 \pm 0.11 \pm 0.16$ mag according to Gibson et al. 2000, but 28.08 ± 0.2 mag according to Saha et al. 1995).

A comprehensive summary of published distances to NGC 5128 is given by Rejkuba (2004). Determinations have been made using Mira variable stars, the TRGB, PNLF and SBF; although NGC 5128 was host to the Type Ia SN1986G, unfortunately the large reddening towards this supernova (Phillips et al. 1999; $E(B-V) = 0.50$) makes a distance from the standard candle estimator unreliable[8]. Using $K-$band data, Rejkuba (2004) derived $\mu_0 = 27.96 \pm 0.11$ mag based on the PL relation for Mira variables (calibrated using a distance modulus to the LMC of 18.50 mag, as in this paper), and $\mu_0 = 27.87 \pm 0.16$ mag based on the TRGB. The latter has been established as a solid standard candle for stars with [Fe/H] < -0.7 (Mould & Kristian 1986; Lee et al. 1993; Madore & Freedman 1995; Sakai et al. 1996); the $I-$band TRGB magnitude for NGC 5128 halo stars has been placed, based on HST data, at $m_{TRGB} = 23.88 \pm 0.1$ mag (Soria et al. 1996; Harris et al. 1999, corrected assuming a foreground extinction $A_I = 0.22$ mag, Schlegel, Finkbeiner & Davis 1998) and $m_{TRGB} = 23.83 \pm 0.05$ mag (Rejkuba et al. 2005 – the value of 24.05 mag quoted in the original paper is uncorrected for extinction). These TRGB magnitudes can be converted to distances using the empirical calibration of the $I-$band tip absolute magnitude, M^{TRGB}, as a function of the stars' metallicity, [Fe/H], derived by Bellazzini et al. (2001) from Galactic globular clusters, with zero point anchored by observations of the globular cluster ωCen. Harris et al. (1999) consider only stars with [Fe/H] < -0.7 in measuring m_{TRGB}. Soria et al. (1996) use stars for which $(V-I) > 1.5$ mag (corresponding to [Fe/H] > -1.68 according to Bellazzini et al. 2001), while the m_{TRGB} determination of Rejkuba et al. (2005) is based on stars with $(V-I) < 1.8$ ([Fe/H] < -1.28). Based on the $(V-I)$ range spanned by the TRGB in the published color magnitude diagrams, we estimate a mean [Fe/H] of -1.2 ± 0.5 for both the Soria et al. (1996) and Harris et al. (1999) data, and -1.4 ± 0.1 for the Rejkuba et al. (2005) data. The Bellazzini et al. calibration then leads to TRGB distances to NGC 5128 of $\mu_0 = 27.91 \pm 0.44$ mag (Soria et al. 1996; Harris et al. 1999), and $\mu_0 = 27.89 \pm 0.16$ mag (Rejkuba et al. 2005), where the errors include a 0.12 mag uncertainty in the zero point of the Bellazzini et al. calibration.

A PNLF distance of $\mu_0^{PNLF} = 27.73^{+0.03}_{-0.05}$ was published by Hui et al. (1995) based on a sample of 224 planetary nebulae. The authors use an empirical calibration of the PNLF based on the Cepheid distance to M31; using the updated calibration by Ferrarese et al. (2000), based on Cepheid distances to six galaxies (including M31) with PNLF measurements, gives $\mu_0^{PNLF} = 27.83^{+0.03}_{-0.05}$. The SBF distance to NGC 5128 is, at the moment, less firmly constrained. In their SBF survey, Tonry et al. (2001) report $\mu_0^{SBF} = 28.12 \pm 0.14$, but two factors have surfaced since which require this distance to be revised. First, the zero point of the SBF distance scale (based on Cepheid distances to the bulges of six spirals with SBF measurements) has been updated (Blakeslee et al. 2002). Adopting the new zero point gives a revised distance modulus $\mu_0^{SBF} = 28.06 \pm 0.14$ mag. Second, new wide-field mosaic observations (Peng et al. 2004; E. Peng, private communication) indicate that the original $(V-I)$ color measured by Tonry et al. (2001) for the bulge of NGC 5128 was significantly underestimated, by approximately 0.07 mag. The revised color is more reasonable for an early-type galaxy of this luminosity. The reason for the unexpectedly large error was the inadequate area available for sky estimation on the small format CCDs used to observe this large galaxy in the ground-based SBF survey. Because the slope of the linear SBF–$(V-I)$ calibration is 4.5, the Tonry et al. SBF distance must be revised further by $4.5 \times 0.07 = 0.32$ mag. With these corrections, the SBF distance modulus becomes $\mu_\circ = 27.74$ mag. The SBF calibration will be revisited in a future contribution comparing SBF and Cepheid distances to NGC4647/NGC4649.

To summarize, distance estimates for NGC 5128 are confined in the very narrow range $\mu_0 = 27.74 \pm 0.14$ (SBF) to $\mu_0 = 27.96 \pm 0.11$ mag (Mira variables, Rejkuba 2004). Our Cepheid distance modulus, $\mu_\circ = 27.67 \pm 0.12$ (random) ± 0.16 (systematic) is consistent with both estimates within the quoted uncertainties.

We conclude by returning briefly to the five *bona-fide* Cepheids which appeared under-luminous in the $P-W$ plot of Figure 9. These objects are identified by the large squares in Figure 7 and correspond to Cepheids C43, C50, C52, C54, and C56 in Table 5. Given the presence of an older stellar population associated with the bulge and halo of NGC 5128, it is not unreasonable to expect the detection of Population II variables, such as RR-Lyrae stars, Anomalous Cepheids, RV Tauri and Pop II Cepheids (themselves divided in BL Herculis for periods between 1 and 8 days, and W Virginis for longer periods) within our WFPC2 field. RR-Lyrae are fainter (by 4 to 6 $V-$band magnitudes) and have shorter variability timescales (< 0.8 day) than any of the variables discussed here; Anomalous Cepheids, which have been detected in a number of dwarf spheroidals (Nemec et al. 1994; Wallerstein 2002) are also not known for periods longer than 1.6 days. RV Tauri stars have characteristic light curves showing alternating deep and shallow minima (see Alcock et al. 1998 for several exceptionally well sampled light curves in the LMC), which are not charac-

[8] Note that the GCLF distance published by Harris et al. (1988) is to be considered tentative since based on a luminosity function which did not reach the turnover; this distance was in fact not used in subsequent papers by some of the authors (e.g. Harris et al. 1999).

teristic of any of the variables in NGC 5128.

The remaining, and indeed likely possibility is that the five under-luminous variables in NGC 5128 are Population II Cepheids of the W Virginis class. These are known to have regular light curves, which compared to those of classical (Pop I) Cepheids, often display a flat maximum, a symmetric minimum and/or a hump during the decline phase (Schmidt et al. 2004; Alcock et al. 1998). Although such differences cannot be easily appreciated in sparsely sampled light curves such as the ones available for NGC 5128, all of the under-luminous variables in NGC 5128, with the exception of C50, show a broad maximum (C43, C52), a symmetric light curve (C54) and/or a slow ascent (C56): in other words, their light curves are consistent with those seen for Pop II Cepheids. In a CMD, Pop II Cepheids occupy the instability strip, and indeed Figure 7 shows that the five under-luminous variables in NGC 5128 do not appear to have abnormal colors (the fact that four of them are among the bluest of the Cepheids discovered in NGC 5128 could simply reflect the fact that they suffer from lower internal extinction, as expected for objects belonging to the bulge or halo). Finally, the under-luminous Cepheids have mean $V-$band magnitudes consistent with those expected based on the PL relation observed by Alcock et al. (1998) for Pop II Cepheids and RV Tauri stars in the LMC (Figure 9)[9].

Beyond the Milky Way globular clusters, bulge and halo, Pop II Cepheids have been detected only in the LMC (Alcock et al. 1998), the Fornax dwarf spheroidal (Bersier & Wood 2002) and, possibly, NGC 6822 (Antonello et al. 2002), IC 1613 (Antonello et al. 1999) and the And I and And III dwarf spheroidal companions of M31 (Pritzl et al. 2005). If our assessment of the under-luminous variables in NGC 5128 is correct, to the best of our knowledge this would represent the first detection of Pop II Cepheids outside the Local group.

The work presented in this paper is based on observations with the NASA/ESA Hubble Space Telescope, obtained by the Space Telescope Science Institute, which is operated by AURA, Inc. under NASA contract No. 5-26555. Support for this work was provided by NASA through grant GO-09043.02 from the Space Telescope Science Institute (STScI).

[9] Unfortunately, the PL relation for Pop II Cepheids is not characterized in the $I-$band.

REFERENCES

Alard, C., & Lupton, R. 1998, ApJ, 503, 325
Alcock, C., et al. 1998, AJ, 115, 1921
Antonello, E., Mantegazza, L., Fugazza, D., & Bossi, M. 1999, A&A, 350, 797
Antonello, E., Fugazza, D., Mantegazza, L., Stefanon, M., & Covino, S. 2002, A&A, 386, 860
Bellazzini, M., Ferraro, F., & Pancino, E. 2001, ApJ, 556, 635
Bersier, D., & Wood, P. R. 2002, AJ, 123, 840
Blakeslee, J. P., Lucey, J. R., Tonry, J. L., Hudson, M. J., Narayanan, V. K., & Barris, B. J. 2002, MNRAS, 330, 443
Cardelli, J.A., Clayton, G.C., & Mathis, J.S. 1989, ApJ, 345, 245
Ciardullo, R., Jacoby, G. H., & Harris, W. E. 1991, ApJ, 383, 487
Ciardullo, R., Feldmeier, J. J., Jacoby, G. H., Kuzio de Naray, R., Laychak, M. B., & Durrell, P. R. 2002, ApJ, 577, 31
Djorgovski, S., & Davis, M. 1987, ApJ, 313, 59
Dolphin, A. E. 2000, PASP, 112, 1397
Dolphin, A. E., et al. 2001, ApJ, 550, 554
Dressler, A., Lynden-Bell, D., Burstein, D., Davies, R. L., Faber, S. M., Terlevich, R., & Wegner, G. 1987, ApJ, 313, 42
Feast, M. W., Glass, I. S., Whitelock, P. A., & Catchpole, R. M. 1989, MNRAS, 241, 375
Ferrarese, L., et al. 1996, ApJ, 464, 568
Ferrarese, L., et al. 2000, ApJ, 529, 745
Freedman, W.L., et al. 1994, ApJ, 427, 628
Freedman, W.L., et al. 2001, ApJ, 553, 47
Gibson, B.K., et al. 2000, ApJ, 529, 723
Harris, W. E., Harris, G. L. H., Holland, S. T., & McLaughlin, D. E. 2002, AJ, 124, 1435
Groenewegen, M. A. T., Romaniello, M., Primas, F., & Mottini, M. 2004, A&A, 420, 655
Harris, H.C., Harris, G.L.H., & Hesser, J.E. 1988, IAUS, 126, 205
Harris, G. L. H., Harris, W. E., & Poole, G. B. 1999, AJ, 117, 855
Heyer, I., et al. 2005, Wide Field and Planetary Camera 2 Instrument Handbook, Version 9.1, STScI publications.
Hill, R., et al. 1998, ApJ, 496, 648
Holtzman, J.A., et al. 1995, PASP, 107, 1065
Hough, J., Bailey, J., Rouse, M, & Whittet, D. 1987, MNRAS, 227, 1P.
Hui, X., Ford, H. C., Freeman, K. C., & Dopita, M. A. 1995, ApJ, 449, 592
Jacoby, G. H., Ciardullo, R., & Feldmeier, J. J. 1999, ASP Conf. Ser. 167: Harmonizing Cosmic Distance Scales in a Post-HIPPARCOS Era, 167, 175
Jordán, A., et al. 2005, ApJ, 634, 1002
Karachentsev, I. D., et al. 2002, A&A, 385, 21
Kelson, D.D., et al. 2000, ApJ, 529, 768
Kennicutt, R. C., et al. 1998, ApJ, 498, 181
Lanoix, P., Paturel, G., & Garnier, R. 1999, Academie des Sciences Comptes Rendus Serie Mecanique Physique Chimie Sciences de la Terre et de l'Univers, 327, 431
Lee, M. G., Freedman, W. L., & Madore, B. F. 1993, ApJ, 417, 553
Luks, Th., & Rohlfs, K. 1992, A&A, 263, 41
Macri, L., et al. 2001, ApJ, 549, 721
Madore, B.F., & Freedman, W.L. 1991, PASP, 103, 933
Madore, B.F., & Freedman, W.L. 1995, AJ, 109, 1645
Madore, B.F., & Freedman, W.L. 1998, in Stellar Astrophysics for the Local Group, ed. A. Aparicio, A. Herrero, & F. Sanchez (New York: Cambridge Univ. Press), 263
Malin, D., Quinn, P., & Graham, J. 1983, ApJ, 272, L5
McCall, M. L. 2004, AJ, 128, 2144
Méndez, B., Davis, M., Moustakas, J., Newman, J., Madore, B. F., & Freedman, W. L. 2002, AJ, 124, 213
Mould, J.R., & Kristian, J. 1986, ApJ, 305, 591
Mould, J.R., et al. 2000a, ApJ, 529, 786
Mould, J.R., et al. 2000b, ApJ, 536, 266
Nemec, J.M., Nemec, A.F.L., & Lutz, T.E. 1994, AJ, 108, 222
Oosterloo, T. A., Morganti, R., Sadler, E. M., Vergani, D., & Caldwell, N. 2002, AJ, 123, 729
Paczynski, B., & Stanek, K. Z. 1998, ApJ, 494, L219
Peng, E. W., Ford, H. C., & Freeman, K. C. 2004, ApJS, 150, 367
Phillips, M. M., Lira, P., Suntzeff, N. B., Schommer, R. A., Hamuy, M., & Maza, J. 1999, AJ, 118, 1766
Phillips, M., et al. 1987, PASP, 99, 839
Pritzl, B. J., Armandroff, T. E., Jacoby, G. H., & Da Costa, G. S. 2005, AJ, 129, 2232
Rejkuba, M. 2004, A&A, 413, 903
Rejkuba, M., Greggio, L., Harris, W. E., Harris, G. L. H., & Peng, E. W. 2005, ApJ, 631, 262
Richtler, T. 2003, in Stellar Candles for the Extragalactic Distance Scale, Eds D. Alloin and W. Gieren, Springer, 635, p.281
Romaniello, M., Primas, F., Mottini, M., Groenwegen, M., Bono, G., & Francois, P. 2005, A&A, 429, L37
Saha, A., & Hoessel, J.G. 1990, AJ, 99, 97
Saha, A., et al. 1994, ApJ, 425, 14
Saha, A., et al. 1995, ApJ, 438, 8

Saha, A., Sandage, A. R., Labhardt, L., Tammann, G. A., Macchetto, F. D., & Panagia, N. 1996, ApJ, 466, 55
Saha, A., Sandage, A., Tammann, G.A., Dolphin, A.E., Christensen, J., Panagia, N., & Macchetto, F.D. 2001, ApJ, 562, 314
Sakai, S., Madore, B.F., & Freedman, W.L. 1986, ApJ, 461, 713
Sakai, S., et al. 2000, ApJ, 529, 698
Sakai, S., Ferrarese, L., Kennicutt, R., and Saha, A. 2004, ApJ, 608, 42
Sandage, A., Saha, A., Tammann, G.A., Panagia, N., & Macchetto, D. 1996, ApJ, 401, L7
Madore, B. F. 1982, ApJ, 253, 575
Schechter, P., Mateo, M., & Saha, A. 1993, PASP, 105, 1342
Schlegel, D.J., Finkbeiner, D.P., & Davis, M. 1998, ApJ, 500, 525
Schmidt, E.G., Johnston, D., Langan, S., Lee, K.M. 2004, AJ, 128, 1748
Soria, R., et al. 1996, ApJ, 465, 79
Stellingwerf, R.F. 1978, ApJ, 224, 953
Stetson, P.B. 1994, PASP, 106, 250
Stetson, P.B. 1996, PASP, 108, 851
Stetson, P.B. 1998, PASP, 110, 1448
Stetson, P.B., et al. 1998, ApJ, 508, 491
Sutherland, R., Bicknell, G., and Dopita, M. 1994, ApJ, 414, 510
Thim, F., Tammann, G. A., Saha, A., Dolphin, A., Sandage, A., Tolstoy, E., & Labhardt, L. 2003, ApJ, 590, 256
Tonry, J.L., & Schneider, P.L. 1988, AJ, 96, 807
Tonry, J. L., Dressler, A., Blakeslee, J. P., Ajhar, E. A., Fletcher, A. B., Luppino, G. A., Metzger, M. R., & Moore, C. B. 2001, ApJ, 546, 681
Udalski, A., Szymanski, M., Kubiak, M., Pietrzynski, G., Soszynski, I., Wozniak, P., & Zebrun, K. 1999, Acta Astron., 49, 201
Udalski, A. 2000, ApJ, 531, L25
van Gorkom, J., van der Hulst, J., Haschick, A. , and Tubbs, A. 1990, AJ, 99, 1781
Wallerstein, G. 2002, PASP, 114, 689
Westerlund, B.E. 1996, The Magellanic Clouds, Cambridge Univ Press, Cambridge

Table 1. Log of Observations.

Date Obs.	HJD (days)	Rootname	Filter	Exp. Time (s)
2001-07-08	2452099.00	u6dm2101r,u6dm2102r	F555W	1200+1100
		u6dm2103r,u6dm2104r	F814W	1300+1100
2001-07-14	2452105.50	u6dm2201r,u6dm2202r	F555W	1300+1300
2001-07-22	2452112.50	u6dm2301r,u6dm2302r	F555W	1300+1300
		u6dm2303r,u6dm2304r	F814W	1300+1400
2001-07-24	2452114.50	u6dm2401r,u6dm2402r	F555W	1300+1300
2001-07-26	2452116.75	u6dm2501r,u6dm2502r	F555W	1300+1300
		u6dm2503r,u6dm2504m	F814W	1300+1400
2001-07-28	2452119.25	u6dm2601r,u6dm2602r	F555W	1300+1300
2001-08-01	2452123.00	u6dm2701m,u6dm2702r	F555W	1300+1300
		u6dm2703r,u6dm2704r	F814W	1300+1400
2001-08-03	2452125.25	u6dm2801r,u6dm2802r	F555W	1300+1300
2001-08-07	2452128.75	u6dm2901m,u6dm2902m	F555W	1300+1300
		u6dm2903m,u6dm2904m	F814W	1300+1400
2001-08-11	2452133.00	u6dm3001m,u6dm3002m	F555W	1300+1300
2001-08-16	2452137.75	u6dm3101m,u6dm3102m	F555W	1300+1300
		u6dm3103m,u6dm3104m	F814W	1300+1400
2001-08-20	2452142.00	u6dm3201m,u6dm3202m	F555W	1300+1300

Table 2. Adopted ALLFRAME Photometric Zero Points (short-exposure).

Chip	Transformation equations
PC	$\mathrm{F555W} = -2.5\log_{10}(\mathrm{DN}/t) + 22.328$
	$\mathrm{F814W} = -2.5\log_{10}(\mathrm{DN}/t) + 21.483$
WF2	$\mathrm{F555W} = -2.5\log_{10}(\mathrm{DN}/t) + 22.388$
	$\mathrm{F814W} = -2.5\log_{10}(\mathrm{DN}/t) + 21.529$
WF3	$\mathrm{F555W} = -2.5\log_{10}(\mathrm{DN}/t) + 22.387$
	$\mathrm{F814W} = -2.5\log_{10}(\mathrm{DN}/t) + 21.505$
WF4	$\mathrm{F555W} = -2.5\log_{10}(\mathrm{DN}/t) + 22.361$
	$\mathrm{F814W} = -2.5\log_{10}(\mathrm{DN}/t) + 21.498$
All	$\mathrm{V} = \mathrm{F555W} - 0.052(V-I) + 0.027(V-I)^2$
	$\mathrm{I} = \mathrm{F814W} - 0.063(V-I) + 0.025(V-I)^2$

Table 3. Comparison of DoPHOT and ALLFRAME Photometry for the Secondary Standard Stars.

Chip	ΔV(DoP.−ALL.) (mag)	ΔI(DoP.−ALL.) (mag)	No. Stars
PC	0.059 ± 0.002	0.031 ± 0.004	36
WF2	0.032 ± 0.002	-0.105 ± 0.002	23
WF3	-0.008 ± 0.001	-0.084 ± 0.001	58
WF4	-0.008 ± 0.001	-0.080 ± 0.001	42

Table 4. Adopted DoPHOT Photometric Zero Points (short-exposure).

Chip	Transformation equations
PC	$\mathrm{F555W} = -2.5\log_{10}(\mathrm{DN}/t) + 1.202$
	$\mathrm{F814W} = -2.5\log_{10}(\mathrm{DN}/t) + 0.324$
WF2	$\mathrm{F555W} = -2.5\log_{10}(\mathrm{DN}/t) + 1.323$
	$\mathrm{F814W} = -2.5\log_{10}(\mathrm{DN}/t) + 0.615$
WF3	$\mathrm{F555W} = -2.5\log_{10}(\mathrm{DN}/t) + 1.345$
	$\mathrm{F814W} = -2.5\log_{10}(\mathrm{DN}/t) + 0.539$
WF4	$\mathrm{F555W} = -2.5\log_{10}(\mathrm{DN}/t) + 1.340$
	$\mathrm{F814W} = -2.5\log_{10}(\mathrm{DN}/t) + 0.530$
All	$\mathrm{V} = \mathrm{F555W} - 0.052(V-I) + 0.027(V-I)^2$
	$\mathrm{I} = \mathrm{F814W} - 0.063(V-I) + 0.025(V-I)^2$

TABLE 5. CEPHEID VARIABLE STARS IN NGC 5128.

ID	X (pixel)	Y (pixel)	RA (J2000) (h:m:s)	Dec (J2000) (°:′:″)	Period (days)	V^{Int} (mag)	I^{Int} (mag)	V^{ph} (mag)	I^{ph} (mag)	Chip
C1	147.2	305.5	13:25:13.534	−43:00:17.05	5.0	25.14	24.12	25.08	24.06	WF2
C2	268.4	201.4	13:25:14.711	−43:00:26.29	5.3	24.61	23.46	24.66	23.52	WF2
C3	129.8	651.9	13:25:13.659	−42:59:04.99	7.0	24.12	23.45	24.08	23.44	WF3
C4	616.0	621.5	13:25:09.448	−42:59:19.04	7.3	23.94	23.18	23.94	23.20	WF3
C5	687.9	358.4	13:25:14.224	−43:01:10.44	7.4	24.98	23.97	24.95	23.92	WF2
C6	547.4	411.9	13:25:18.163	−43:00:11.80	8.2	24.86	23.66	24.86	23.67	PC
C7	603.4	611.7	13:25:09.578	−42:59:19.68	8.6	23.99	22.94	24.04	22.94	WF3
C8	590.3	683.2	13:25:18.589	−43:00:23.32	8.8	24.93	23.38	24.88	23.36	PC
C9	775.3	498.0	13:25:13.184	−43:01:22.05	9.4	24.16	22.94	24.11	22.93	WF2
C10	410.4	552.9	13:25:19.519	−42:59:14.54	10.6	23.98	22.95	23.98	22.96	WF4
C11	126.2	587.3	13:25:13.827	−42:59:11.10	11.0	23.84	23.01	23.84	23.00	WF3
C12	440.9	478.7	13:25:18.802	−42:59:13.22	11.2	23.60	22.70	23.60	22.70	WF4
C13	713.1	536.5	13:25:18.945	−43:00:15.57	12.7	25.43	23.54	25.38	23.54	PC
C14	317.6	562.9	13:25:19.794	−42:59:23.31	12.7	23.99	22.93	23.92	22.92	WF4
C15	473.8	318.7	13:25:17.778	−43:00:08.44	12.8	24.64	23.22	24.66	23.21	PC
C16	422.6	403.3	13:25:18.171	−42:59:16.66	13.9	23.27	22.40	23.31	22.41	WF4
C17	478.9	162.1	13:25:15.929	−42:59:16.53	13.9	23.64	22.61	23.64	22.60	WF4
C18	158.0	229.3	13:25:14.227	−43:00:16.31	14.3	24.08	22.88	24.03	22.85	WF2
C19	294.3	754.6	13:25:21.524	−42:59:21.32	14.9	23.41	22.36	23.41	22.42	WF4
C20	646.7	305.9	13:25:18.462	−43:00:06.09	15.1	23.86	22.80	23.87	22.83	PC
C21	336.9	589.5	13:25:19.990	−42:59:20.85	15.1	23.73	22.80	23.68	22.79	WF4
C22	715.0	716.8	13:25:08.390	−42:59:12.20	15.5	23.76	22.58	23.77	22.55	WF3
C23	487.8	491.5	13:25:10.845	−42:59:28.62	16.1	25.03	23.15	25.05	23.16	WF3
C24	170.5	267.1	13:25:13.922	−43:00:18.39	16.5	23.91	22.80	23.91	22.79	WF2
C25	139.5	600.2	13:25:10.924	−43:00:23.27	16.5	24.73	22.97	24.74	22.98	WF2
C26	503.2	215.1	13:25:16.346	−42:59:13.00	16.6	23.35	22.36	23.34	22.35	WF4
C27	123.3	617.8	13:25:10.736	−43:00:22.13	17.3	24.74	23.24	24.73	23.25	WF2
C28	429.5	755.4	13:25:21.260	−42:59:08.25	17.9	23.71	22.62	23.71	22.61	WF4
C29	382.8	574.6	13:25:11.667	−43:00:46.11	20.5	23.94	22.45	23.85	22.44	WF2
C30	657.0	337.8	13:25:18.533	−43:00:07.39	20.9	24.21	22.81	24.23	22.83	PC
C31	421.0	589.1	13:25:11.230	−42:59:17.66	21.3	23.57	22.44	23.51	22.42	WF3
C32	422.6	123.5	13:25:12.191	−43:00:02.65	22.2	24.05	22.62	24.10	22.63	WF3
C33	728.9	50.2	13:25:17.005	−43:01:07.04	22.4	23.38	22.27	23.30	22.25	WF2
C34	65.7	233.4	13:25:15.097	−42:59:43.83	22.5	24.59	22.86	24.63	22.90	WF3
C35	698.1	198.6	13:25:18.565	−43:00:00.84	22.6	24.93	22.89	24.91	22.91	PC
C36	474.8	288.4	13:25:17.050	−42:59:14.13	23.1	23.01	22.10	22.96	22.07	WF4
C37	423.5	369.9	13:25:17.875	−42:59:17.31	23.1	22.98	21.77	23.02	21.76	WF4
C38	295.2	696.4	13:25:12.113	−42:59:04.46	24.1	23.27	22.22	23.34	22.26	WF3
C39	94.6	539.4	13:25:14.205	−42:59:15.00	26.4	23.32	22.22	23.30	22.21	WF3
C40	320.7	632.0	13:25:12.024	−42:59:11.23	27.1	23.35	22.28	23.33	22.27	WF3
C41	755.1	554.5	13:25:08.370	−42:59:28.69	27.8	23.67	22.33	23.67	22.32	WF3
C42	476.9	78.9	13:25:15.202	−42:59:18.55	30.5	23.34	22.14	23.35	22.15	WF4
C43	222.6	215.3	13:25:13.761	−42:59:49.21	34.1	24.77	24.02	24.77	24.02	WF3
C44	500.9	439.6	13:25:10.838	−42:59:33.94	34.7	24.26	22.24	24.25	22.23	WF3
C45	257.6	387.2	13:25:13.095	−42:59:33.41	41.2	23.74	21.92	23.73	21.91	WF3
C46	474.9	106.9	13:25:15.981	−43:00:43.99	42.8	24.43	22.33	24.41	22.31	WF2
C47	475.5	338.9	13:25:17.804	−43:00:09.32	≥44.0	23.37	21.59	23.35	21.58	PC
C48	500.2	114.7	13:25:15.967	−43:00:46.62	≥44.0	24.44	22.42	24.42	22.42	WF2
C49	85.1	98.6	13:25:16.166	−42:59:55.92	44.4	23.12	21.70	23.13	21.69	WF4
C50	275.9	341.2	13:25:13.495	−43:00:30.28	47.0	24.32	23.32	24.27	23.29	WF2
C51	348.4	695.1	13:25:11.648	−42:59:05.80	≥48.0	25.11	22.92	25.10	22.92	WF3
C52	341.9	450.9	13:25:12.669	−43:00:39.25	≥48.5	25.06	24.05	24.96	24.02	WF2
C53	544.7	440.4	13:25:18.254	−42:59:04.00	48.5	22.27	21.34	22.33	21.37	WF4
C54	439.2	668.6	13:25:17.968	−43:00:24.26	≥50.4	23.59	22.70	23.55	22.68	PC
C55	599.0	480.1	13:25:18.496	−42:58:57.88	≥74.0	24.98	22.75	25.02	22.76	WF4
C56	604.1	670.5	13:25:20.163	−42:58:53.25	≥80.0	24.11	22.88	24.12	22.89	WF4

NOTE. — Cepheids are numbered in order of increasing period. X and Y positions are in the reference frame of the first exposure, u6dm2101r (see Table 1). Columns 7 and 8 give intensity-averaged V and I magnitudes respectively (equation 3), while columns 9 and 10 give phase-weighted magnitudes (equation 4) assuming the period listed in column 6. The last column lists the chip in which the Cepheid is located.

Table 6. Cepheid Distance Estimates to NGC 5128.

Case	Sample	No. Cepheids	μ_V (mag)	μ_I (mag)	$E(V-I)$ (mag)	$R_V^{NGC5128} = 3.3$ μ_0 (mag)	$R_V^{NGC5128} = 3.3$ d (Mpc)	$R_V^{NGC5128} = 2.4$ μ_0 (mag)	$R_V^{NGC5128} = 2.4$ d (Mpc)
1	All Chips, Ceph. only, P≥8d, Ph.Mag.	42	28.85 ± 0.10	28.30 ± 0.06	0.55 ± 0.05	27.48 ± 0.05	3.1 ± 0.1	27.62 ± 0.04	3.4 ± 0.1
2	All Chips, Ceph. only, P≥15d, Ph.Mag.	28	29.02 ± 0.12	28.43 ± 0.06	0.59 ± 0.07	27.54 ± 0.07	3.2 ± 0.1	27.70 ± 0.05	3.5 ± 0.1
3	All Chips, Ceph. only, P≥20d, Ph.Mag.	19	29.09 ± 0.15	28.47 ± 0.07	0.61 ± 0.09	27.55 ± 0.09	3.2 ± 0.1	27.72 ± 0.06	3.5 ± 0.1
4	All Chips, Ceph. only, P≥25d, Ph.Mag.	9	29.22 ± 0.21	28.57 ± 0.08	0.65 ± 0.14	27.59 ± 0.14	3.3 ± 0.2	27.77 ± 0.10	3.6 ± 0.2
5	All Chips, Ceph. only, P≥30d, Ph.Mag.	6	29.41 ± 0.29	28.63 ± 0.11	0.78 ± 0.19	27.45 ± 0.19	3.1 ± 0.3	27.68 ± 0.13	3.4 ± 0.2
6	PC, P≥8d, Ph.Mag.	7	29.34 ± 0.21	28.51 ± 0.10	0.83 ± 0.13	27.27 ± 0.14	2.9 ± 0.2	27.52 ± 0.11	3.2 ± 0.2
7	WF2, P≥8d, Ph.Mag.	8	29.14 ± 0.24	28.30 ± 0.15	0.84 ± 0.12	27.05 ± 0.12	2.6 ± 0.1	27.30 ± 0.10	2.9 ± 0.1
8	WF3, P≥8d, Ph.Mag.	13	28.99 ± 0.18	28.31 ± 0.09	0.67 ± 0.10	27.30 ± 0.11	2.9 ± 0.1	27.50 ± 0.08	3.2 ± 0.1
9	WF4, P≥8d, Ph.Mag.	14	28.35 ± 0.09	27.98 ± 0.07	0.37 ± 0.04	27.42 ± 0.07	3.0 ± 0.1	27.50 ± 0.07	3.2 ± 0.1
10	All Chips, Ceph.+Var., P≥8d, Ph.Mag.	70	28.93 ± 0.10	28.39 ± 0.07	0.55 ± 0.05	27.56 ± 0.07	3.3 ± 0.1	27.71 ± 0.07	3.5 ± 0.1

Note. — All distance moduli are based on short-exposure zero points (see § 3.3)

TABLE 7. ERROR BUDGET IN THE DISTANCE TO NGC 5128.

Systematic Uncertainties	$\delta\mu_0$ (mag)	Notes
a) WFPC2 V band zero point	±0.02	
b) WFPC2 I band zero point	±0.01	
c) $V-$band Short to Long Exposure Zero Point Uncertainty	±0.05	
d) $I-$band Short to Long Exposure Zero Point Uncertainty	±0.05	
e) Charge Transfer Efficiency	±0.01	
A) Cumulative Error on μ_V: $\sqrt{a^2+c^2+e^2}$	±0.05	(1)
B) Cumulative Error on μ_I: $\sqrt{b^2+d^2+e^2}$	±0.05	(1)
C) Error on μ_0 due to A and B: $\sqrt{A^2\times(1-R)^2+B^2\times R^2}$	±0.13	(2,3)
i) Error on LMC Distance Modulus	±0.10	
Final Systematic Error on μ_0 due to C and i: $\sqrt{C^2+i^2}$	$\pm$ **0.16**	(1)

Random Uncertainties	$\delta\mu_0$ (mag)	Notes
f) Error on μ_0 due to R_V for NGC 5128:	±0.077	(3)
g) Error on μ_0 due to A_V of LMC:	±0.007	(3)
D) Error on μ_0 due to f and g: $\sqrt{f^2+g^2}$	±0.08	(1)
h) Error on μ_0 due to Metallicity:	±0.08	
j) Random Error on μ_0 from fitting the PL relation (from Table 6):	±0.04	
Final Random Error on μ_0 due to D, h, and j: $\sqrt{D^2+h^2+j^2}$	$\pm$**0.12**	(1)

NOTE. — (1): the errors are uncorrelated, and therefore summed in quadrature. (2): R is defined as $A(V)/E(V-I)=2.143$, according to the extinction law by Cardelli, Clayton and Mathis (1989) for $R_V(NGC5128)=2.4$. (3) The expression for the error is derived from equation (8), assuming that the errors are uncorrelated.

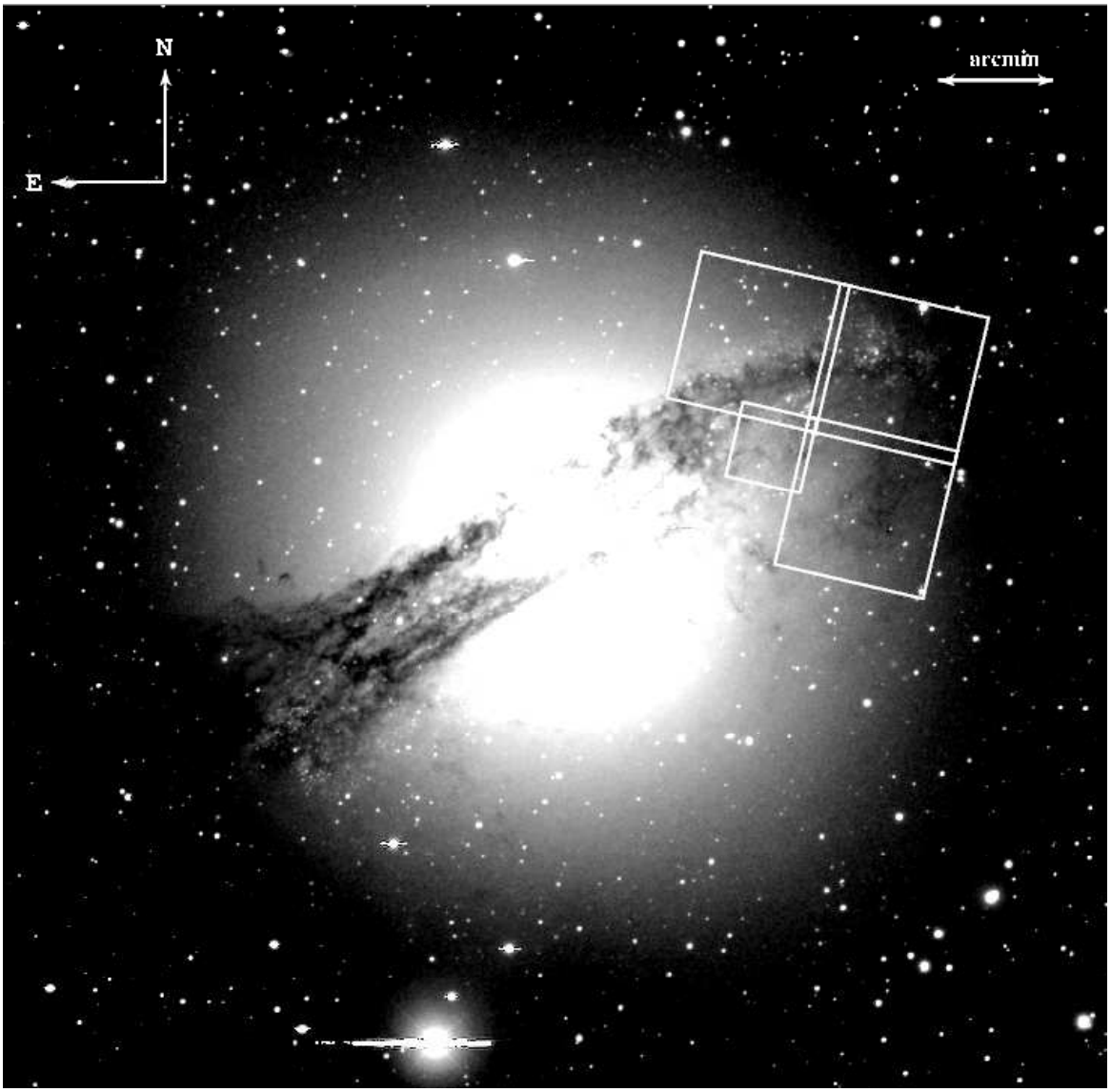

FIG. 1.— A ground based image of NGC 5128, taken with the Prime Focus 8K Mosaic CCD Imager at the CTIO 4.0 meter Victor M. Blanco telescope (courtesy of Holland Ford and Eric Peng). The footprint of the HST/WFPC2 detectors is shown, with the PC having the smaller field of view, and the WF2, WF3 and WF4 detectors arranged in a counter-clockwise fashion following the PC. The image is shown with a logarithmic gray-scale.

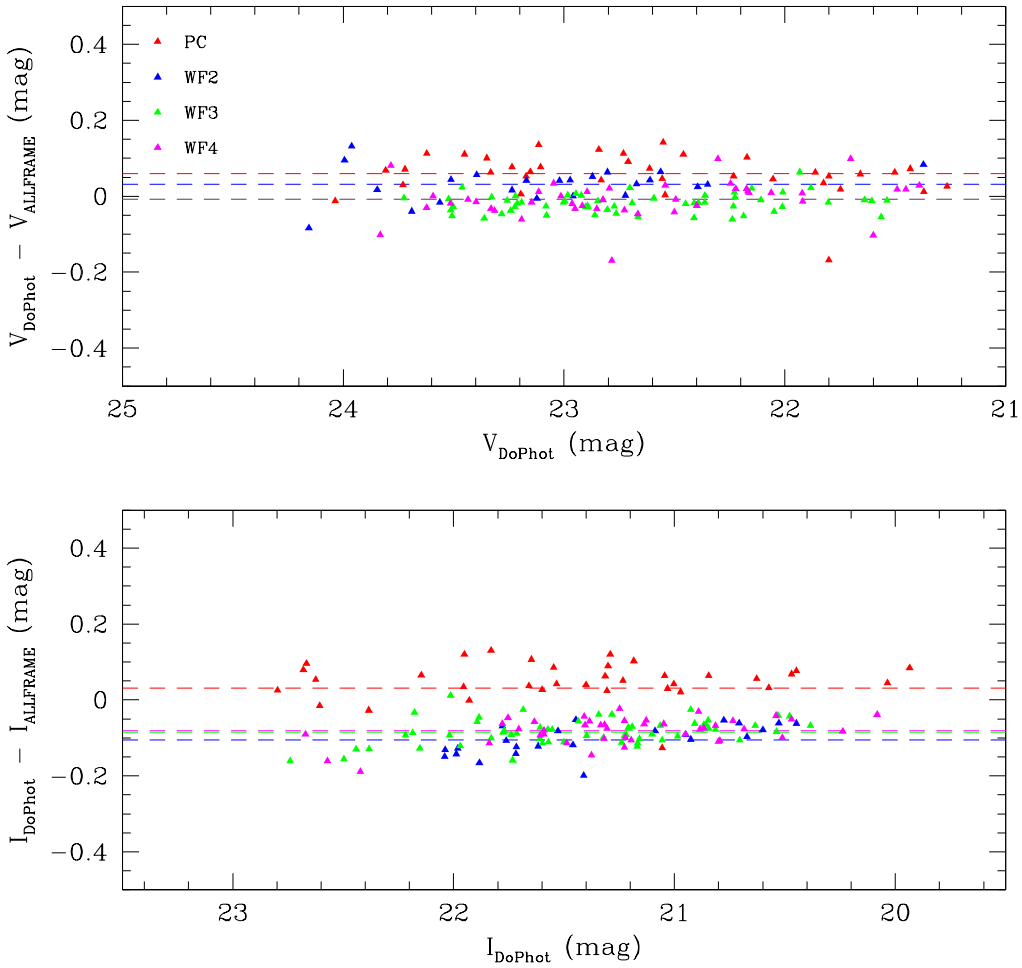

FIG. 2.— Comparison between the V and I DoPHOT and ALLFRAME photometry for the secondary standard stars listed in Table 7. The photometric calibration listed in Table 2 has been adopted for ALLFRAME, while the DoPHOT calibration follows the short exposure zero points of Hill et al. (1998). The mean differences between the DoPHOT and ALLFRAME photometry (shown for each chip by the dashed lines) are listed in Table 3. See text for further details.

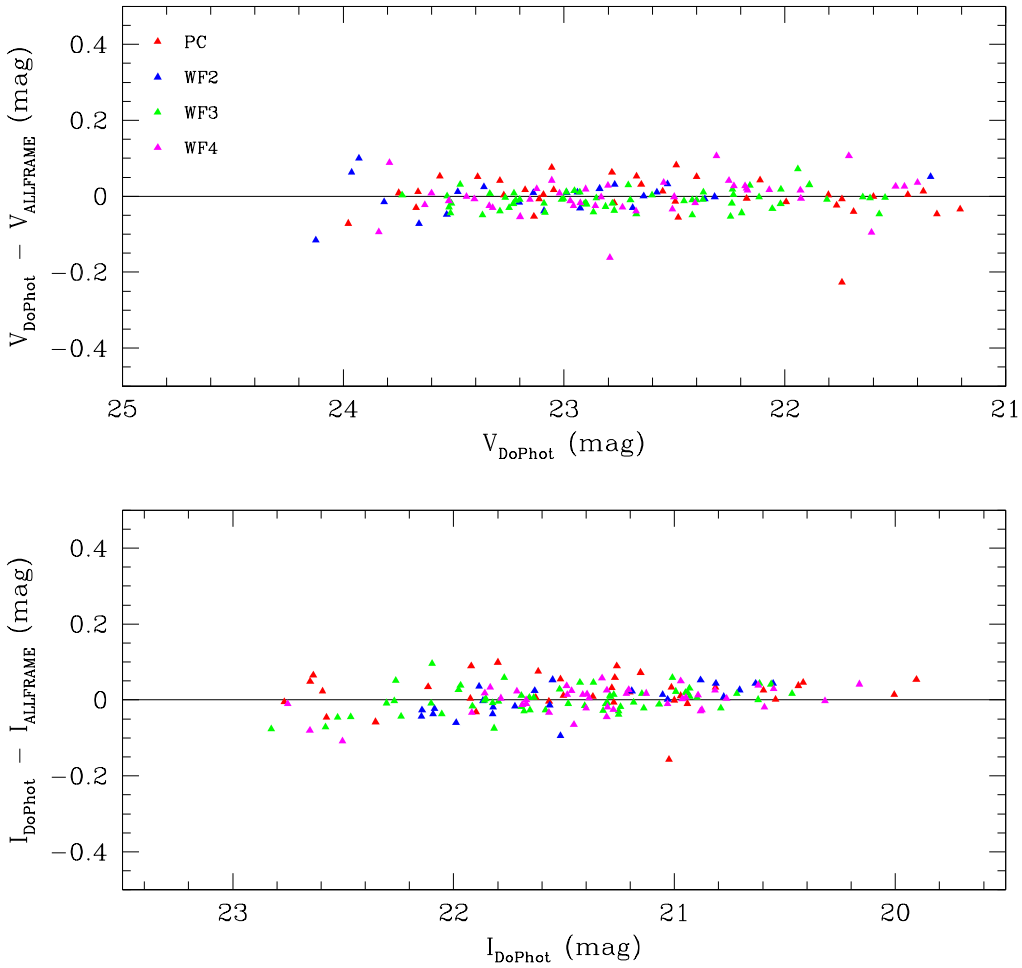

FIG. 3.— Comparison between the V and I DoPHOT and ALLFRAME photometry for the secondary standard stars listed in Table 7, using the photometric calibrations given in Tables 2 and 4.

FIG. 4.— NOTE: Figure 4 can be found on the version of the paper available at http://astrowww.phys.uvic.ca∼lff/publications.html. A deep image, obtained by combining all F555W exposures, showing the PC field of view. To give a sense of the dynamic range spanned by the four chips, the logarithmic gray-scale is kept the same in this figure and the next three figures, showing the WF2, WF3 and WF4 fields of view respectively. All images are shown with the center of the WFPC2 pyramid on the lower left corner; the direction of the North is also marked (as customary, East is 90° counter-clockwise from North). Cepheids are identified by open circles and labeled with the IDs listed in Table 5. Squares identify probable variable stars and are labeled with the IDs listed in Table 10.

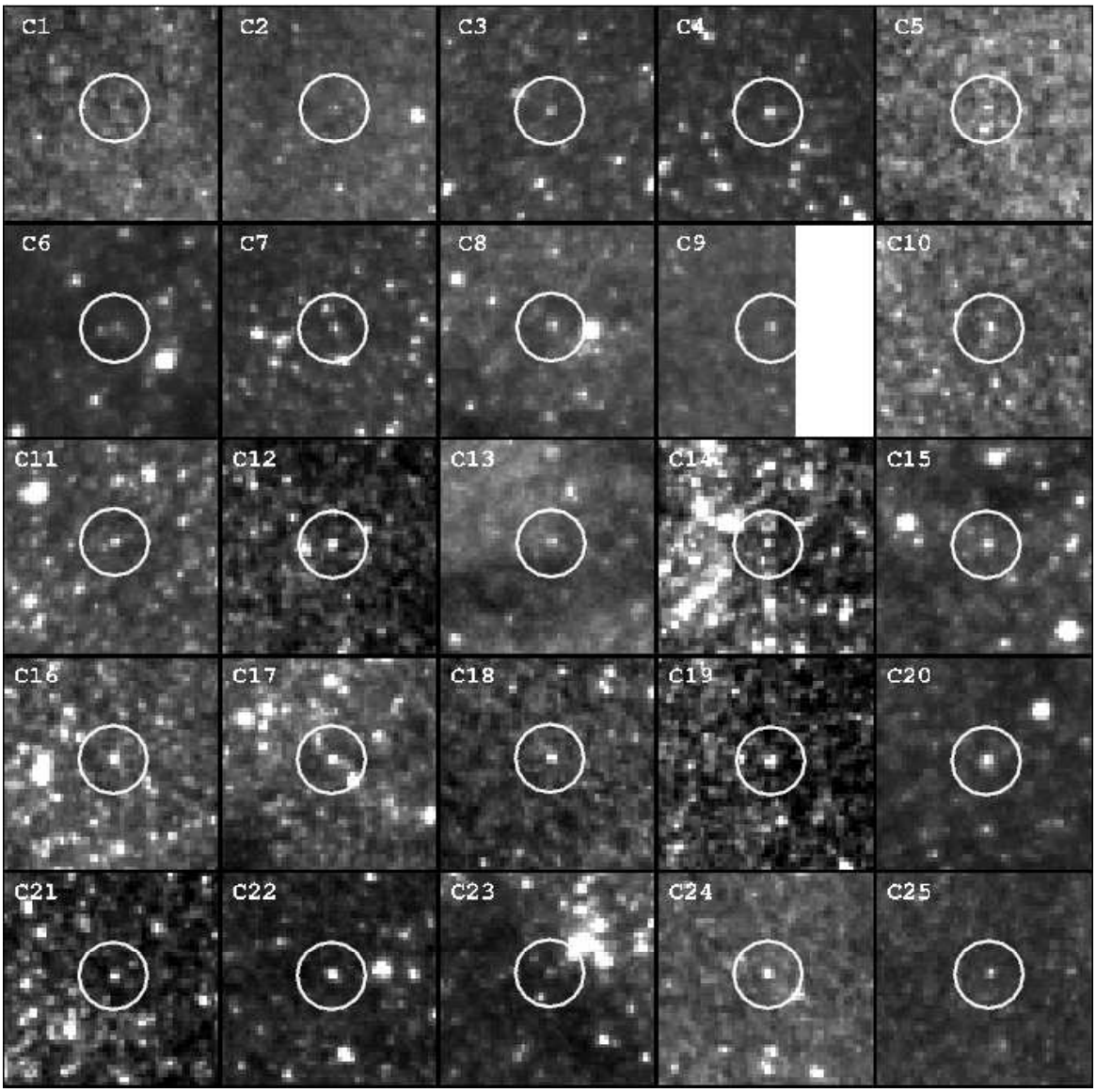

FIG. 5.— Finding charts for the confirmed Cepheids in NGC 5128. The fields shown are $5''\times5''$ for the WF chips, and $2''.5\times2''.5$ for the PC; the orientation of each finding chart is the same as that of the chip to which it belongs, as shown in Figure 4. The gray-scale is different for each finding chart. The Cepheids are numbers following the IDs listed in Table 5.

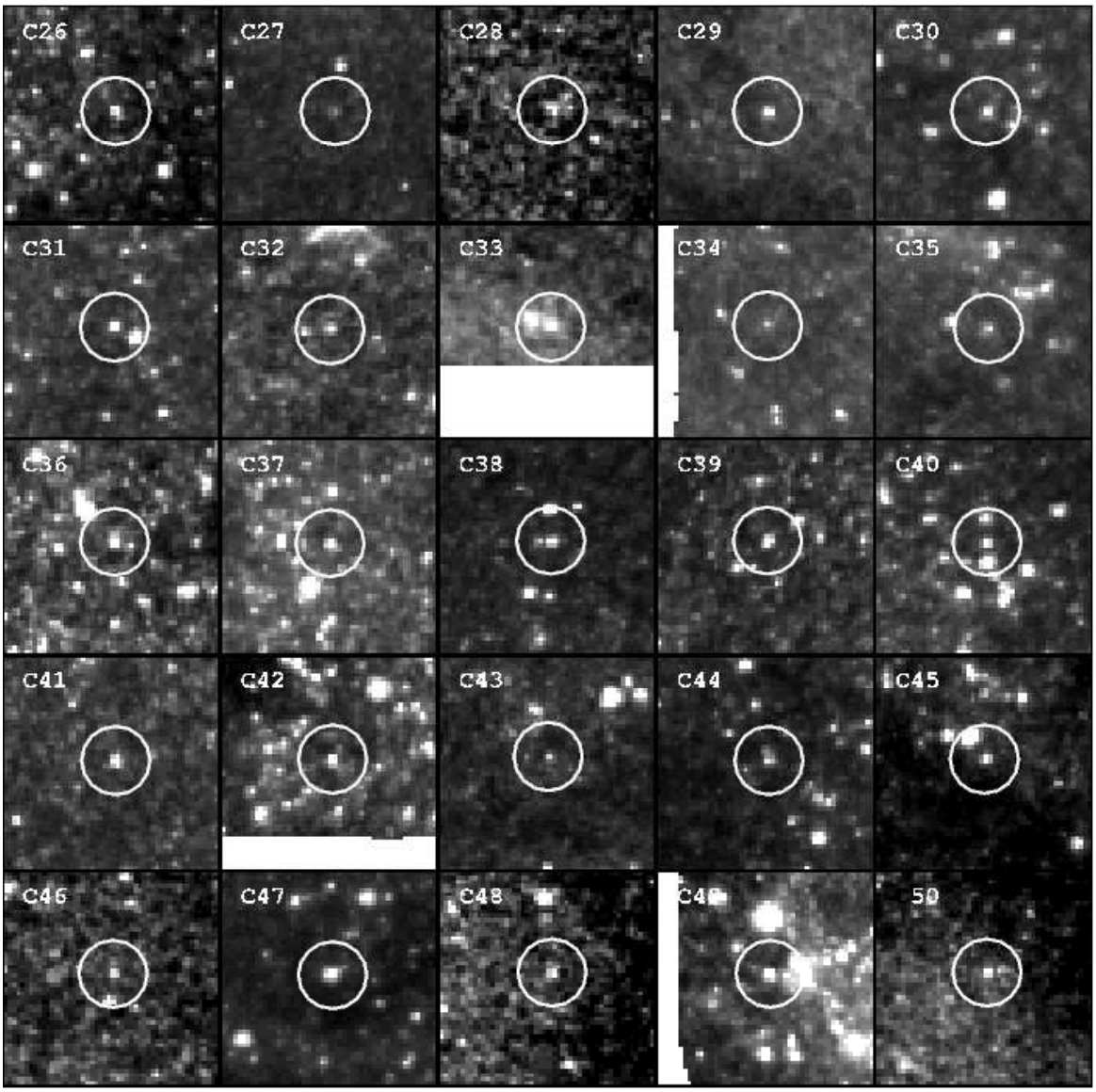

FIG. 5.— Continued.

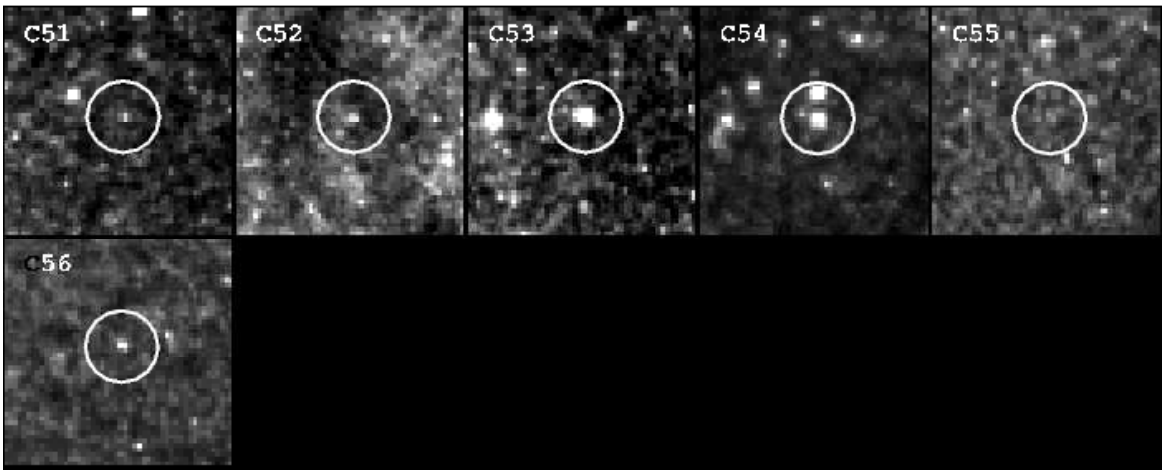

FIG. 5.— Continued.

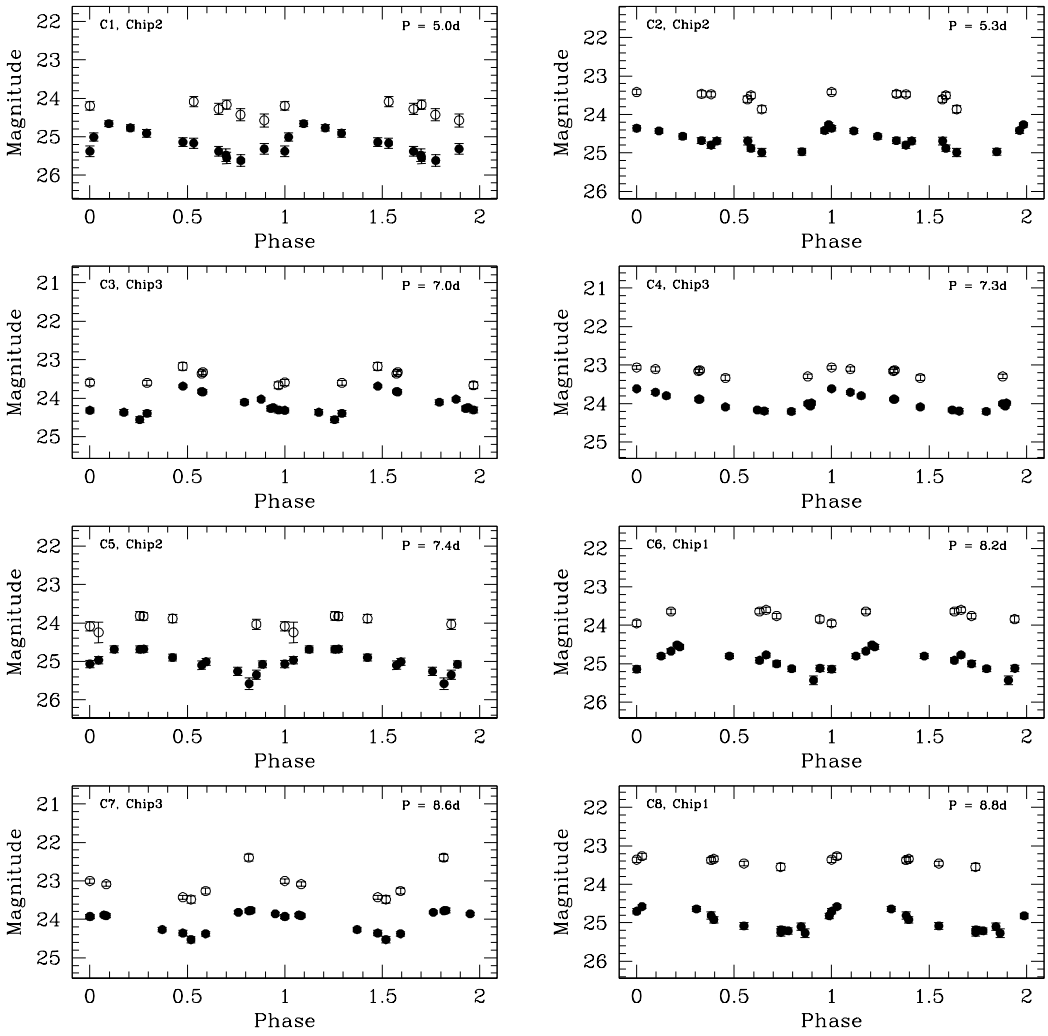

FIG. 6.— Light curves for the NGC 5128 Cepheids, numbered as in Figure 4 and Table 5. The DoPHOT photometry is shown; solid and open circles represent the F555W and F814W data respectively. The period used in phasing the light curves is listed in the upper right corner of each panel as well as in Table 5.

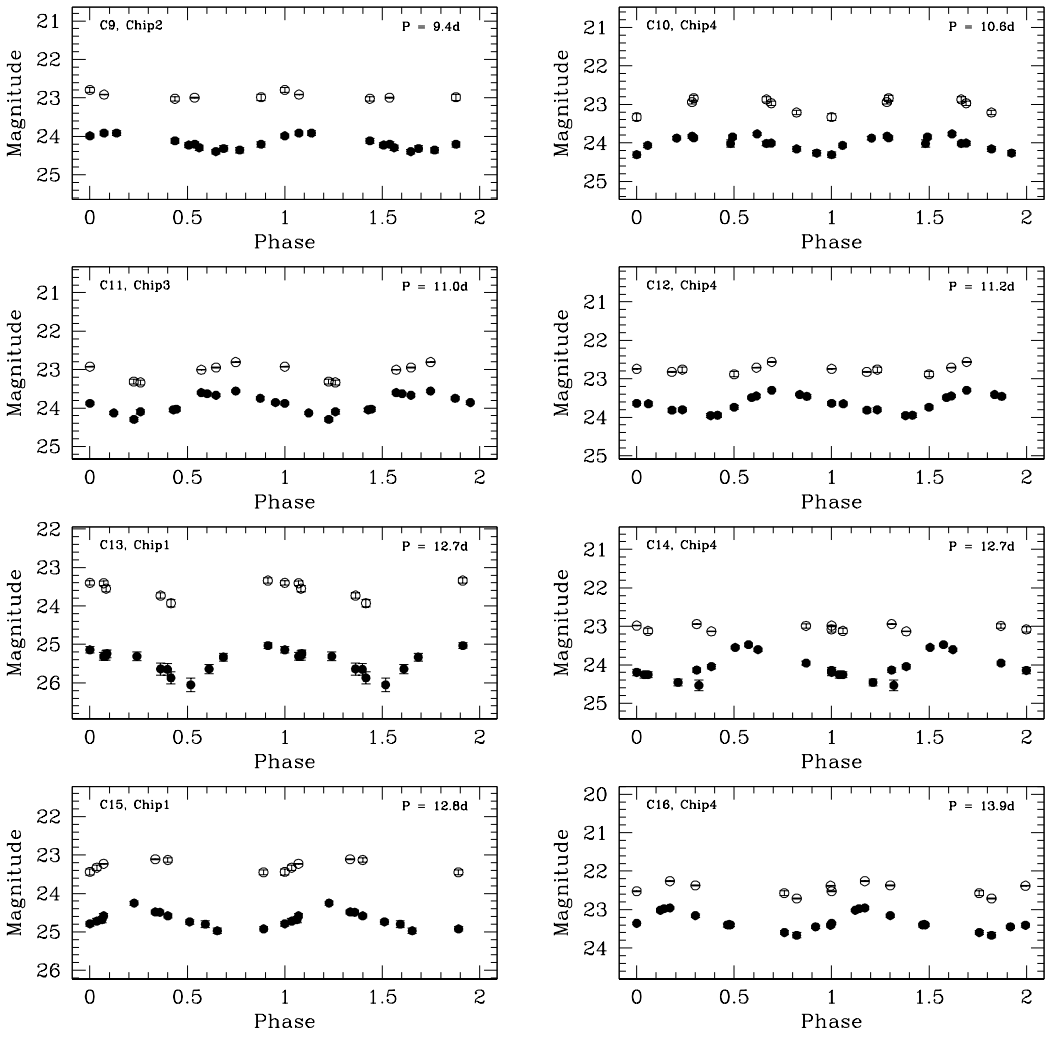

FIG. 6.— Continued.

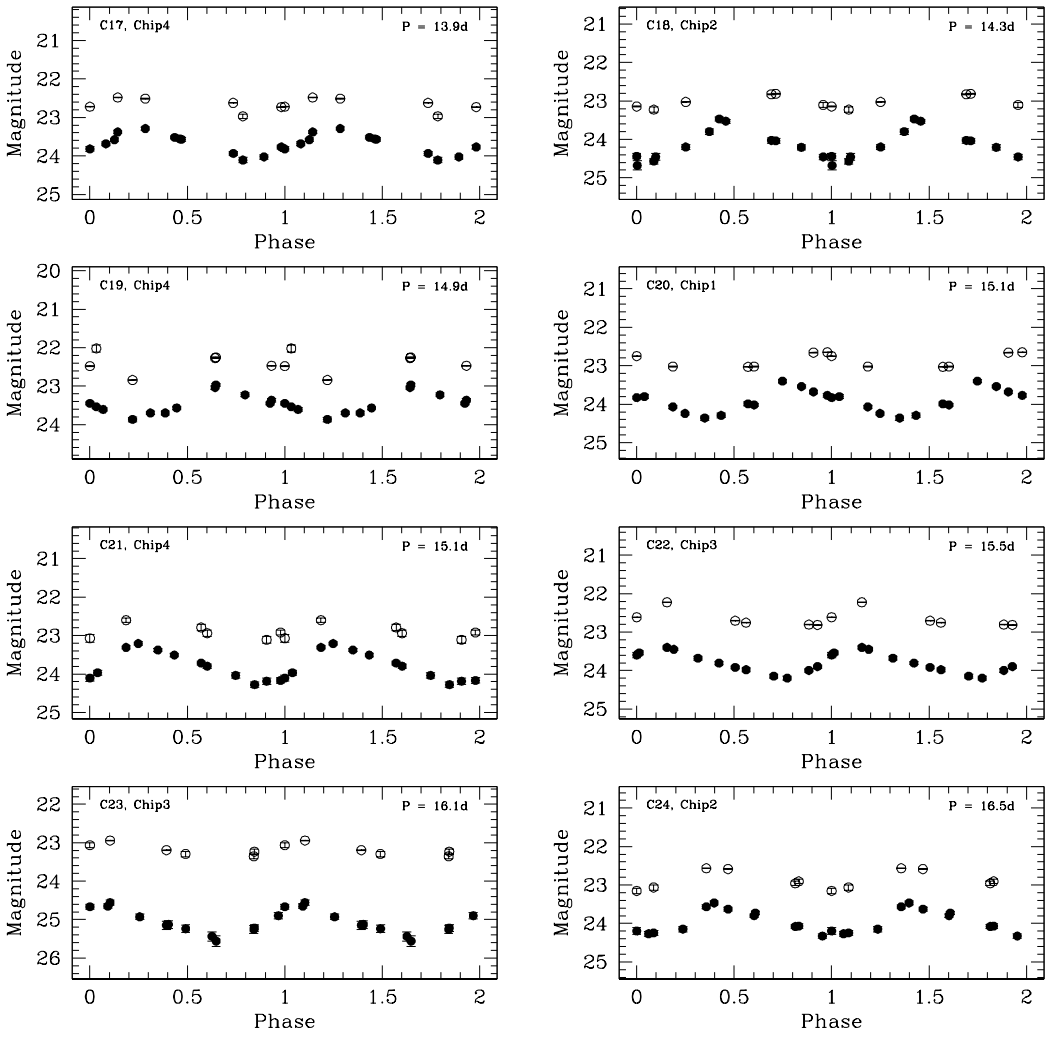

FIG. 6.— Continued.

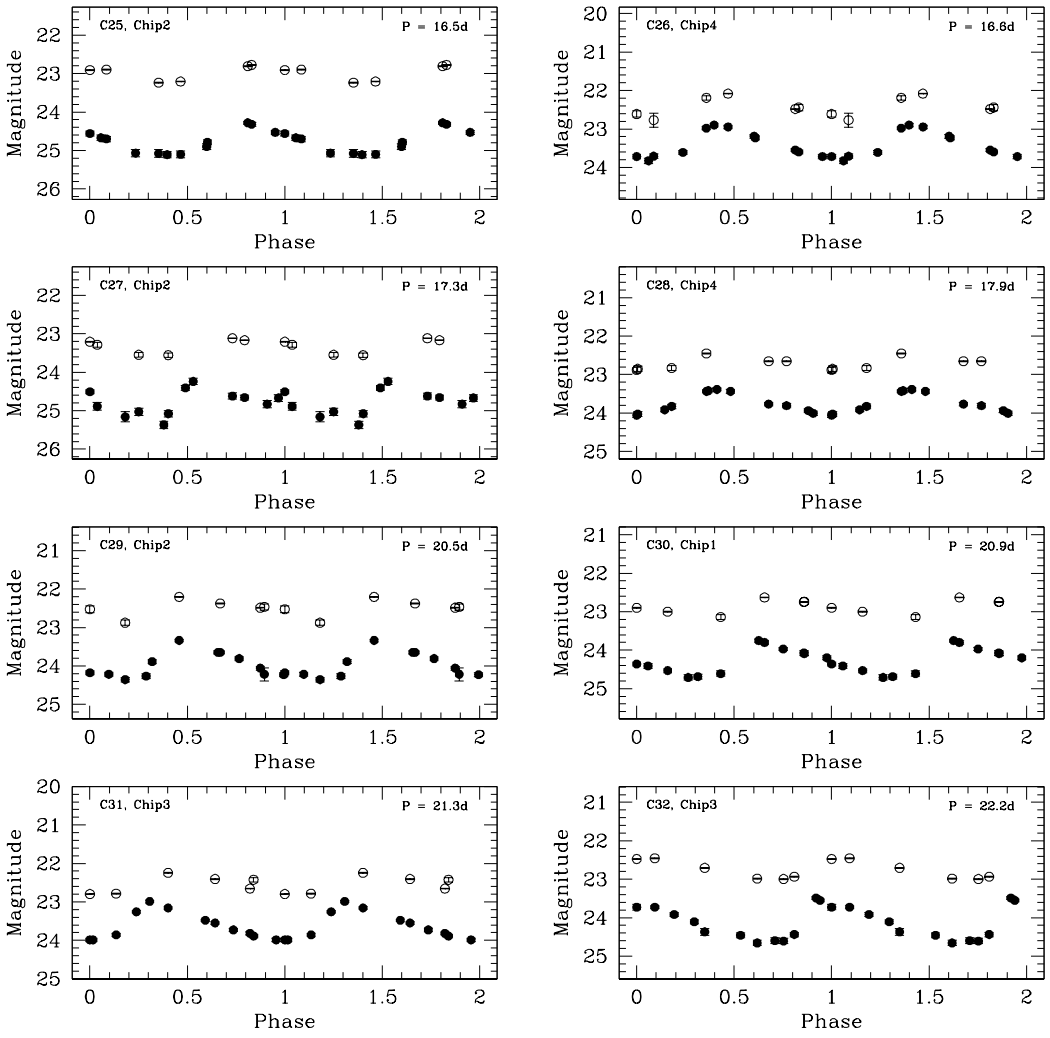

FIG. 6.— Continued.

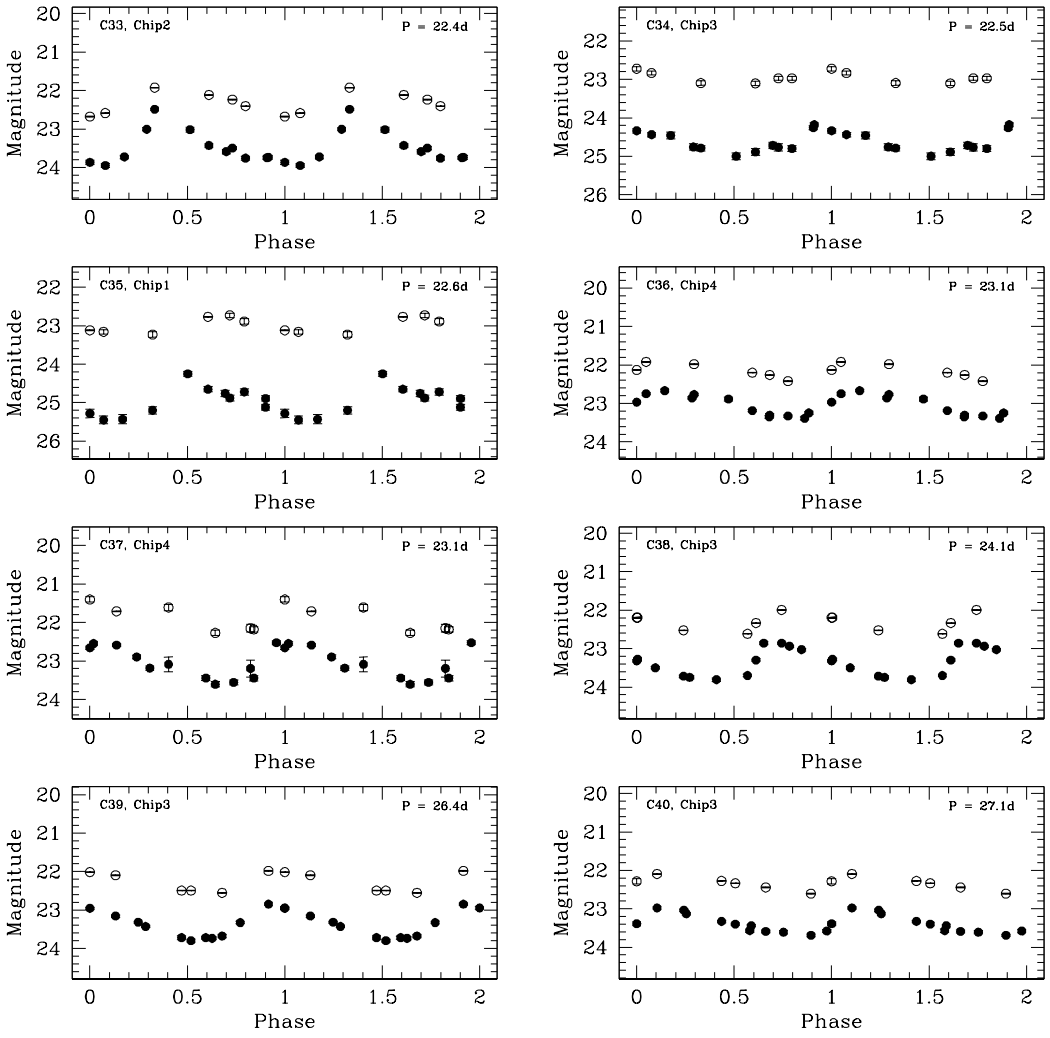

FIG. 6.— Continued.

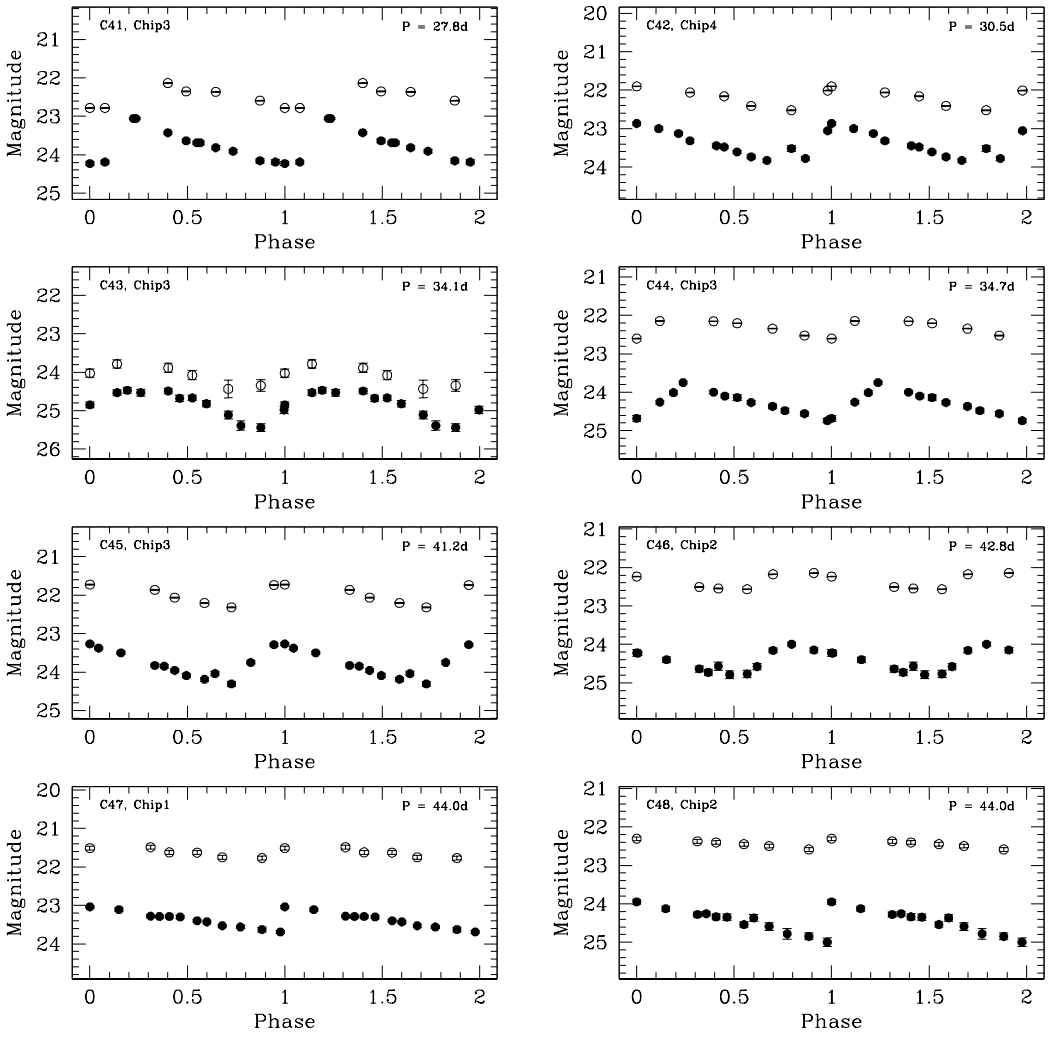

FIG. 6.— Continued.

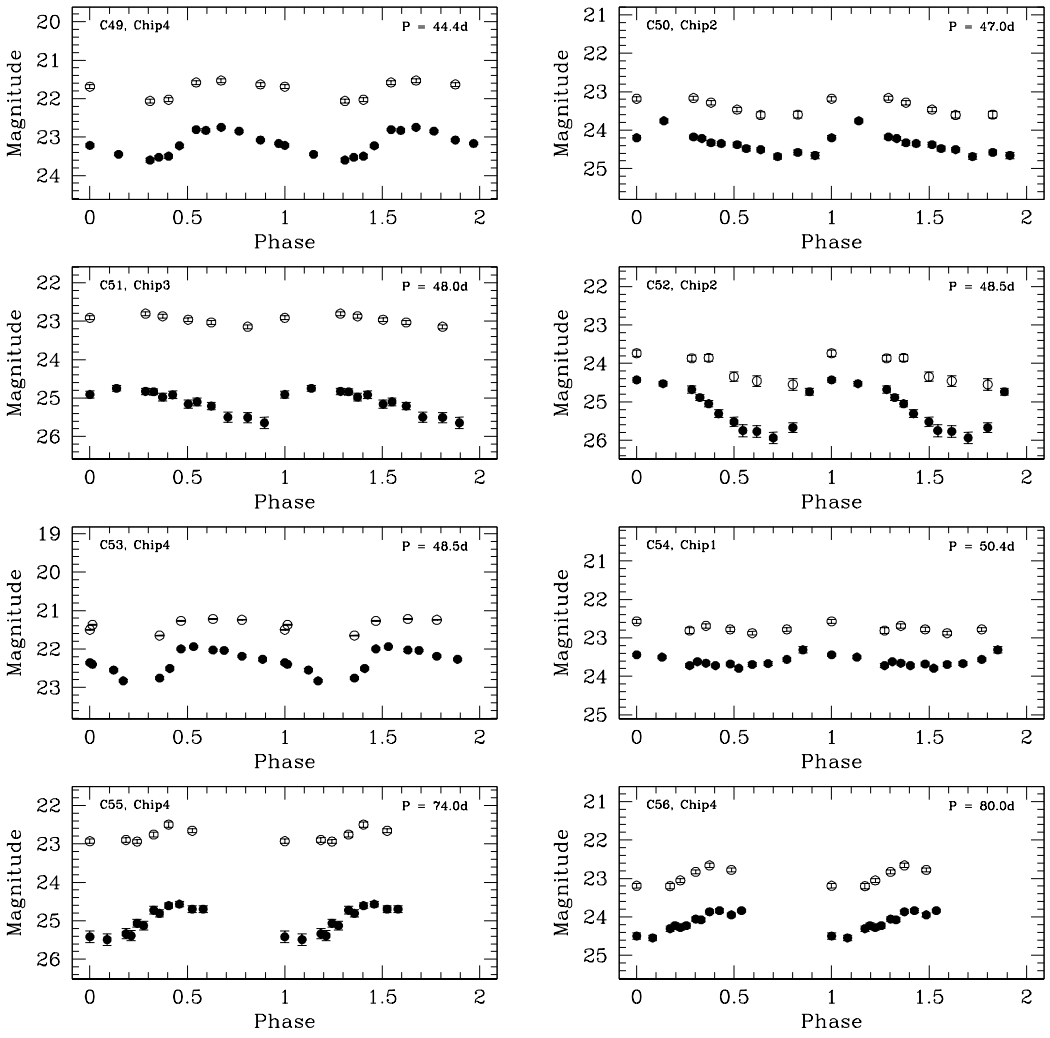

FIG. 6.— Continued.

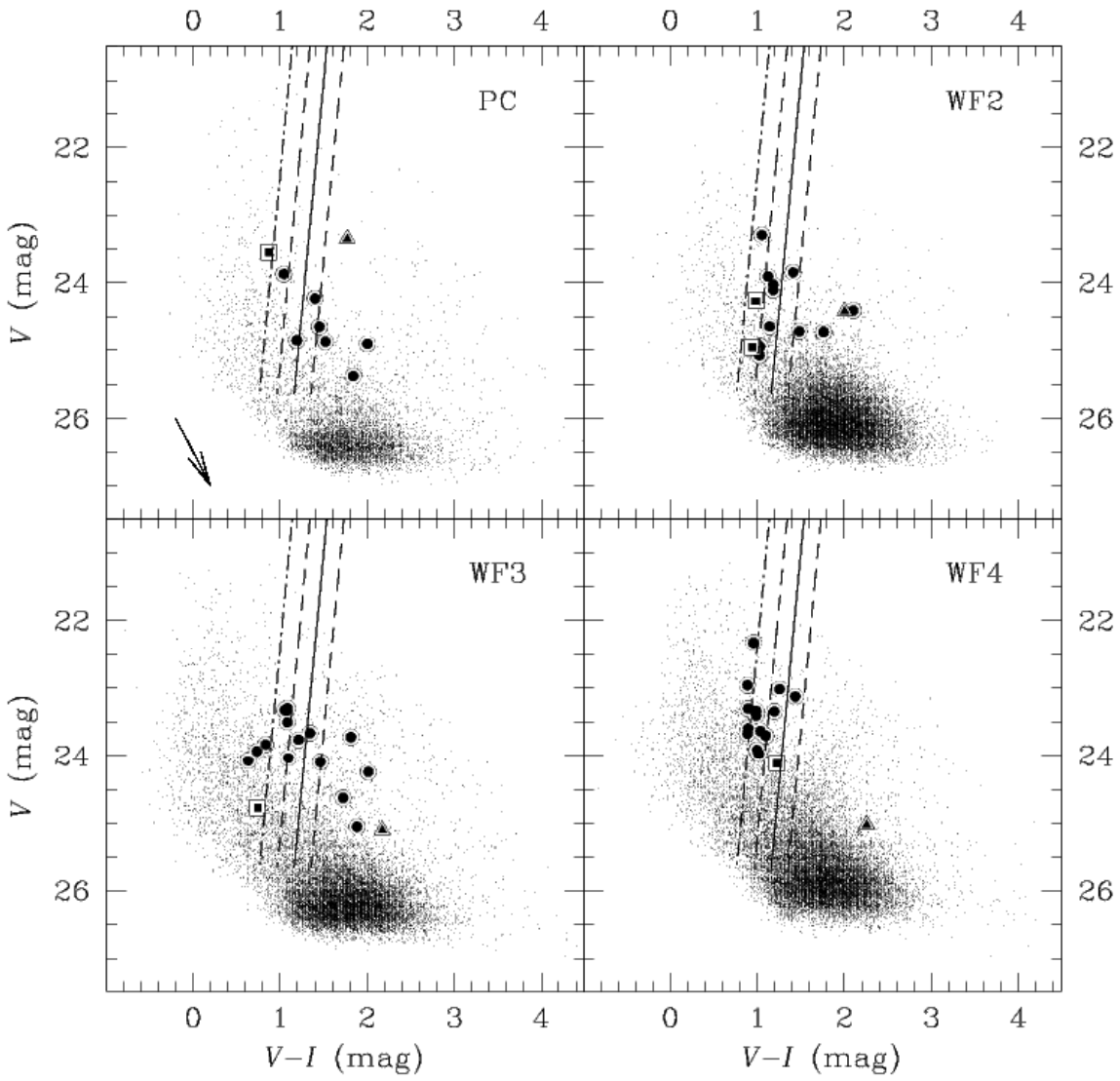

FIG. 7.— V, $V-I$ Color-Magnitude diagrams for NGC 5128, shown separately for each WFPC2 chip. Cepheids used in fitting the PL relation are identified by large circles, while Cepheids for which only a lower limit on the period could be placed are plotted as triangles. The squares identify the Population II Cepheids discussed in the text. The solid line shows the ridge-line of the Cepheid instability strip, with width marked by the dashed lines, assuming a $V-$band distance modulus of 28.85 mag and reddening $E(V-I) = 0.55$ mag (see §5). The dot-dashed line shows the main ridgeline of the instability strip assuming $E(V-I) = 0.152$ mag which, being equal to the Galactic reddening along the line of sight to NGC 5128, represents a lower limit to the amount of total reddening to the Cepheids. The arrow in the upper right panel shows where a star would move if subject to one magnitude of visual extinction (for $R_V = 3.3$). The data are consistent with the assumption that Cepheids lie outside the instability strip as a consequence of the large and highly position dependent reddening of the NGC 5128 field.

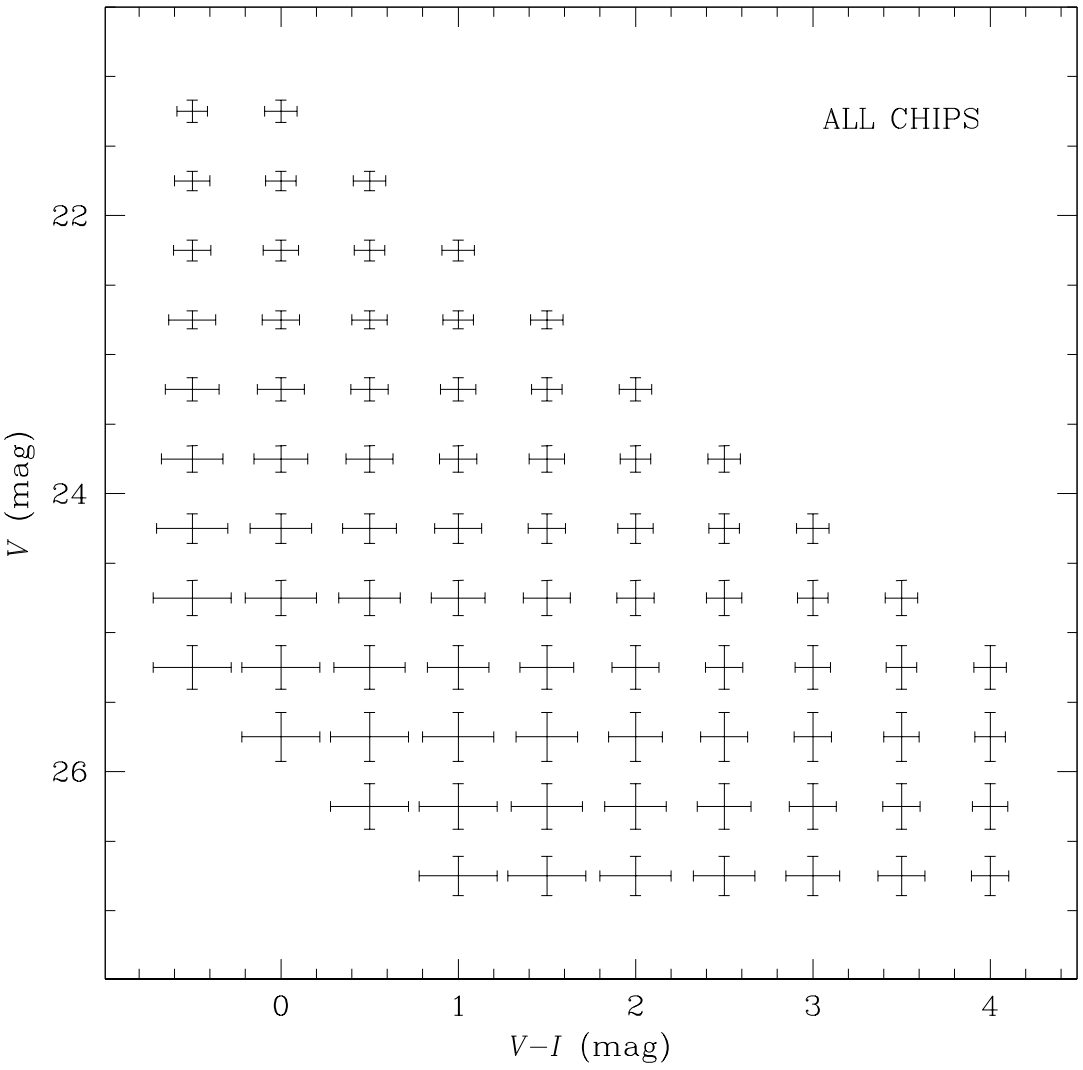

FIG. 8.— Mean photometric errors associated with the DoPHOT photometry, as a function of V, $V-I$. The mean is calculated in 0.5 magnitudes bins, for both V and I.

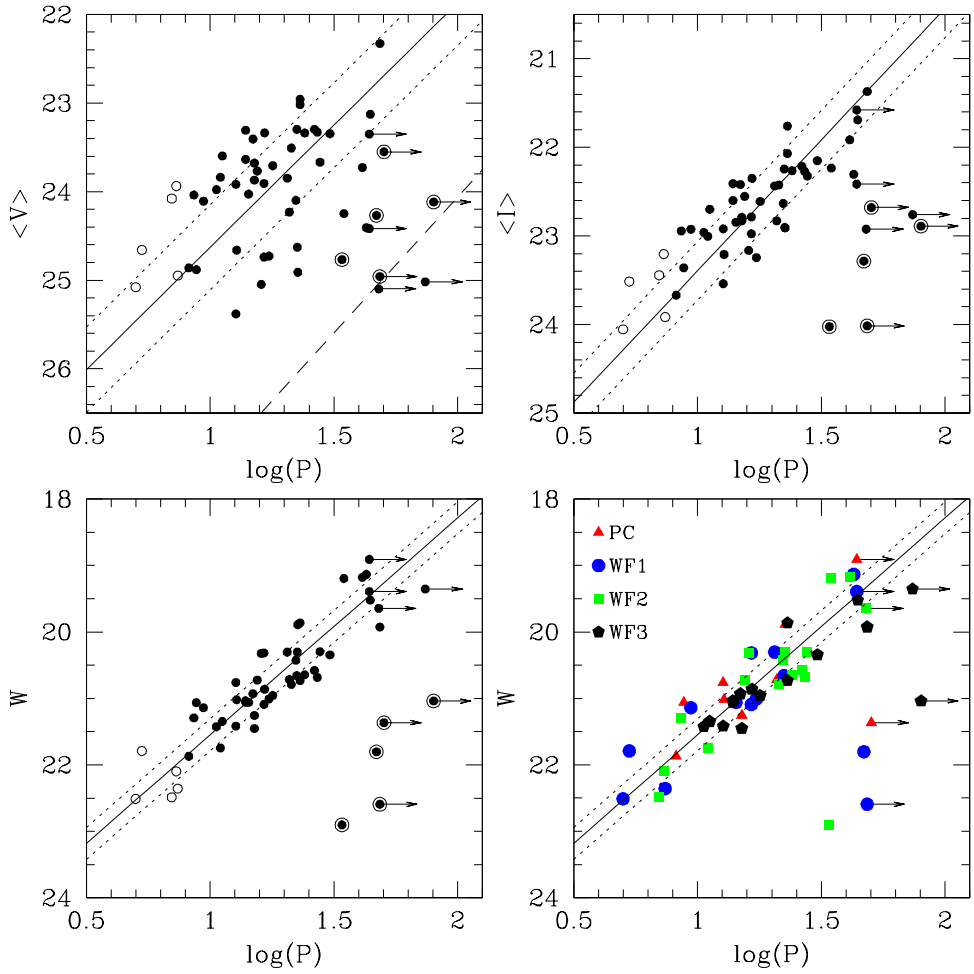

FIG. 9.— V, I, and W Period-Luminosity relations for the NGC 5128 Cepheids. Magnitudes are DoPHOT phase-weighted mean magnitudes. Cepheids plotted as open circles have period less than 8 days, and were excluded from the fits. Cepheids plotted as solid circles surrounded by a larger open circle, which are identified in the text as Pop II Cepheids, deviate by more than 6σ (two times the width of the instability strip) from the main ridge-line, and were also excluded from the fits. Periods of Cepheids plotted as a circle plus an arrow should be considered lower limits. In the bottom right panel, Cepheids are separated according to the chips in which they were detected. W is calculated assuming R_V(LMC)=R_V(N5128)=3.3. The solid lines represent the Cepheids PL relations with slopes fixed at the LMC value, and scaled to μ_V = 28.85 mag; μ_I = 28.30 mag, and μ_0 = 27.48 mag (Table 6). The 3σ confidence limit on these PL relations are shown by the dotted lines. The dashed line in the $V-$band PL relation shows the PL relation for Pop II Cepheids in the LMC from Alcock et al. (1998), scaled to μ_V = 28.85 mag. The 3σ confidence limit on this relation (not shown) is 1.32 mag.

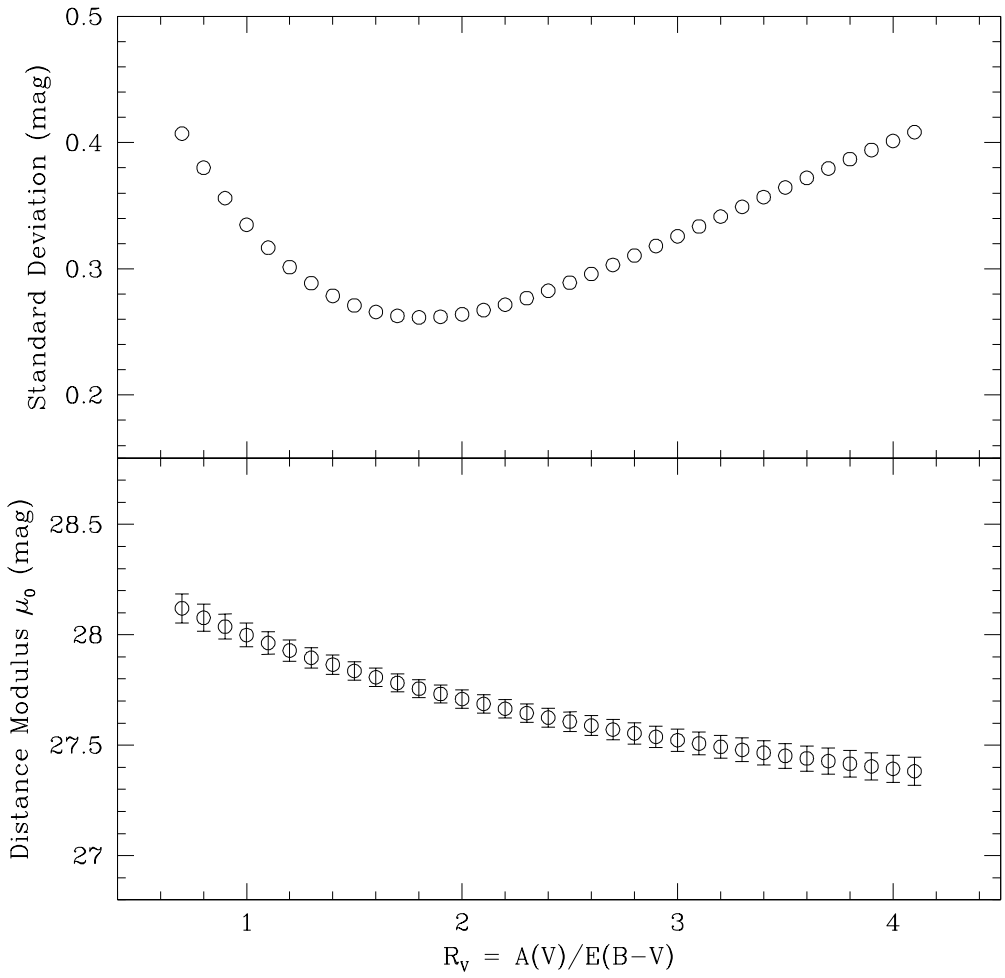

FIG. 10.— Distance modulus (bottom panel) and standard deviation from the best fitting W PL relation (upper panel) as a function of the R_V value assumed for NGC 5128. See text for further details.

Appendix

Table 8. Secondary Standard Stars in NGC 5128.

Chip	X (pix)	Y (pix)	V (mag)	I (mag)
PC	673.4	236.3	21.24± 0.01	19.99± 0.02
PC	340.5	500.6	21.44± 0.01	20.37± 0.02
PC	331.1	540.7	21.36± 0.01	20.40± 0.02
PC	565.5	164.0	21.36± 0.01	20.54± 0.02
PC	150.0	415.8	22.41± 0.01	19.85± 0.02
PC	515.7	703.4	21.75± 0.01	20.98± 0.02
PC	715.9	300.4	22.62± 0.01	20.57± 0.02
PC	511.4	745.1	22.07± 0.01	21.17± 0.02
PC	279.3	142.1	21.97± 0.01	21.18± 0.02
PC	408.1	645.1	21.60± 0.01	21.21± 0.02
PC	678.8	225.7	21.73± 0.01	21.36± 0.02
PC	298.5	365.9	21.79± 0.01	21.25± 0.02
PC	193.0	397.4	22.51± 0.01	21.28± 0.02
PC	459.9	595.8	22.35± 0.01	21.46± 0.02
PC	261.3	331.0	22.01± 0.01	21.49± 0.02
PC	492.3	298.7	22.18± 0.01	21.46± 0.02
PC	726.0	108.4	21.80± 0.02	21.62± 0.02
PC	412.7	405.0	22.54± 0.01	21.57± 0.02
PC	400.3	433.3	23.09± 0.01	21.08± 0.03
PC	421.6	631.2	23.34± 0.02	20.78± 0.02
PC	599.1	682.0	22.62± 0.01	21.70± 0.02
PC	504.2	607.9	22.79± 0.01	21.83± 0.02
PC	659.1	317.3	22.54± 0.01	21.93± 0.02
PC	391.1	467.7	23.25± 0.01	21.54± 0.03
PC	376.0	129.1	23.65± 0.02	20.96± 0.02
PC	275.3	155.9	23.70± 0.02	21.00± 0.02
PC	494.4	141.5	23.19± 0.01	21.92± 0.02
PC	337.3	413.1	23.74± 0.02	21.18± 0.02
PC	106.8	295.2	22.72± 0.02	22.08± 0.03
PC	643.5	701.9	23.03± 0.01	22.57± 0.02
PC	537.4	723.2	22.98± 0.02	22.57± 0.03
PC	524.3	387.2	23.12± 0.02	22.41± 0.02
PC	362.9	725.9	24.05± 0.02	20.95± 0.02
PC	380.0	517.5	23.27± 0.01	22.62± 0.02
PC	164.7	545.7	23.51± 0.02	22.60± 0.03
PC	235.9	573.1	23.16± 0.01	22.77± 0.03
WF2	497.4	557.0	21.31± 0.01	18.84± 0.07
WF2	393.2	187.3	21.81± 0.01	19.86± 0.02
WF2	525.7	776.4	21.33± 0.02	20.29± 0.03
WF2	525.0	312.4	21.29± 0.01	20.77± 0.02
WF2	148.8	393.7	22.31± 0.01	20.28± 0.02
WF2	488.5	731.1	22.67± 0.01	20.32± 0.02
WF2	683.0	401.1	22.32± 0.01	21.03± 0.02
WF2	250.3	559.1	22.96± 0.01	20.68± 0.02
WF2	130.9	486.5	22.98± 0.01	20.59± 0.02
WF2	442.2	380.1	22.50± 0.01	21.50± 0.02
WF2	168.5	765.4	23.34± 0.01	21.17± 0.02
WF2	263.0	729.6	22.74± 0.01	21.86± 0.02
WF2	764.6	214.0	22.72± 0.02	21.85± 0.02
WF2	124.6	628.2	23.47± 0.02	20.77± 0.02
WF2	533.2	344.2	22.37± 0.01	22.05± 0.02
WF2	414.4	154.8	22.57± 0.01	21.87± 0.02
WF2	229.6	356.1	23.22± 0.02	21.61± 0.02
WF2	497.8	309.1	23.58± 0.02	20.51± 0.02
WF2	77.4	277.6	23.23± 0.02	21.67± 0.02
WF2	616.0	201.5	22.82± 0.01	22.11± 0.02
WF2	366.8	525.0	23.13± 0.01	21.84± 0.02
WF2	450.3	426.3	22.93± 0.01	22.19± 0.03
WF2	542.5	762.1	22.64± 0.01	22.13± 0.02
WF2	638.5	96.3	23.83± 0.02	21.04± 0.02
WF2	283.7	634.5	23.90± 0.02	21.58± 0.02
WF2	550.5	234.8	23.13± 0.02	22.17± 0.02
WF2	367.0	718.8	23.73± 0.02	21.74± 0.02
WF2	304.5	534.0	23.83± 0.02	21.61± 0.02
WF2	299.3	306.8	24.24± 0.02	20.83± 0.02
WF3	141.4	721.0	21.62± 0.01	21.13± 0.02
WF3	189.3	181.9	22.22± 0.01	20.62± 0.02
WF3	273.9	191.0	22.12± 0.01	20.81± 0.02
WF3	360.0	576.9	22.04± 0.01	21.19± 0.02
WF3	672.6	632.0	21.62± 0.01	21.28± 0.02
WF3	611.8	244.4	22.84± 0.01	20.45± 0.02
WF3	464.3	452.7	22.43± 0.01	21.61± 0.02
WF3	596.9	512.9	22.26± 0.01	21.71± 0.02

TABLE 8. SECONDARY STANDARD STARS IN NGC 5128.— *Continued*

Chip	X (pix)	Y (pix)	V (mag)	I (mag)
WF3	507.5	578.6	22.81± 0.01	21.28± 0.02
WF3	249.7	189.8	23.01± 0.01	21.08± 0.02
WF3	361.6	298.8	22.86± 0.01	21.32± 0.02
WF3	466.0	247.2	22.93± 0.01	21.29± 0.02
WF3	251.6	290.7	22.23± 0.01	21.86± 0.02
WF3	368.3	256.3	23.02± 0.01	21.35± 0.02
WF3	178.7	710.5	22.24± 0.01	21.93± 0.02
WF3	370.2	650.5	22.41± 0.01	22.21± 0.02
WF3	759.7	178.5	23.21± 0.01	20.95± 0.02
WF3	657.5	229.4	23.23± 0.01	21.32± 0.02
WF3	491.1	319.6	23.13± 0.01	21.49± 0.02
WF3	592.8	80.0	22.92± 0.02	22.09± 0.03
WF3	663.5	289.6	23.44± 0.01	20.57± 0.02
WF3	243.1	740.8	23.33± 0.01	21.26± 0.02
WF3	644.5	204.5	23.53± 0.01	20.52± 0.02
WF3	312.6	417.3	23.59± 0.01	20.16± 0.02
WF3	337.2	699.8	23.53± 0.01	21.65± 0.02
WF3	351.3	717.9	23.55± 0.01	21.83± 0.02
WF3	560.3	137.1	23.28± 0.01	22.51± 0.03
WF3	568.5	341.3	23.25± 0.01	22.31± 0.02
WF3	253.9	391.8	21.87± 0.01	20.90± 0.02
WF3	351.7	379.5	21.55± 0.01	21.26± 0.02
WF3	618.6	371.9	21.86± 0.01	20.97± 0.02
WF3	600.0	384.5	22.78± 0.01	20.13± 0.02
WF3	606.4	403.8	23.03± 0.01	20.28± 0.02
WF3	551.7	455.8	22.38± 0.01	20.92± 0.02
WF3	435.6	544.7	22.80± 0.01	20.89± 0.02
WF3	167.4	449.3	22.57± 0.01	19.95± 0.02
WF3	73.0	386.6	21.65± 0.02	21.38± 0.03
WF3	129.1	705.8	22.30± 0.01	20.92± 0.02
WF3	98.1	633.0	23.42± 0.01	20.70± 0.02
WF3	471.8	596.2	23.56± 0.02	21.16± 0.02
WF3	568.0	597.1	22.92± 0.01	21.28± 0.02
WF3	511.7	597.6	22.60± 0.01	22.57± 0.02
WF3	634.1	591.4	22.41± 0.01	20.26± 0.02
WF3	702.0	549.8	22.71± 0.01	21.95± 0.02
WF3	694.4	539.0	23.22± 0.01	21.42± 0.02
WF3	201.0	770.0	22.91± 0.01	21.49± 0.02
WF3	154.6	695.0	22.47± 0.01	21.71± 0.02
WF3	294.5	703.8	22.72± 0.01	22.27± 0.02
WF3	481.2	697.7	22.98± 0.01	21.31± 0.02
WF3	500.5	777.9	22.13± 0.01	21.93± 0.02
WF3	503.5	768.7	21.82± 0.01	21.68± 0.02
WF3	726.1	718.1	22.00± 0.01	21.80± 0.02
WF3	772.2	487.8	22.36± 0.01	21.63± 0.02
WF3	618.2	568.7	22.47± 0.01	22.28± 0.02
WF3	611.2	431.6	22.68± 0.01	21.85± 0.02
WF3	388.1	560.3	22.09± 0.01	21.89± 0.02
WF3	349.8	396.0	23.33± 0.01	20.93± 0.02
WF3	466.3	265.5	22.92± 0.01	22.90± 0.03
WF3	418.9	349.2	22.94± 0.01	22.65± 0.03
WF3	476.0	354.3	23.27± 0.01	21.71± 0.02
WF3	578.6	367.2	23.11± 0.01	22.11± 0.02
WF3	353.5	156.5	23.73± 0.02	21.68± 0.02
WF3	93.9	70.3	22.24± 0.02	22.00± 0.05
WF4	514.1	201.0	22.42± 0.01	20.61± 0.01
WF4	524.8	439.4	21.47± 0.01	20.58± 0.02
WF4	544.7	440.4	22.20± 0.06	21.27± 0.05
WF4	469.6	370.9	21.36± 0.01	20.52± 0.01
WF4	305.8	368.9	21.43± 0.01	20.76± 0.02
WF4	456.4	662.0	22.05± 0.01	21.45± 0.02
WF4	501.2	149.1	21.91± 0.01	21.30± 0.02
WF4	129.8	366.8	21.93± 0.01	21.69± 0.02
WF4	418.8	228.7	21.60± 0.01	21.11± 0.02
WF4	702.2	139.3	22.32± 0.01	19.68± 0.01
WF4	351.2	324.6	22.50± 0.01	20.03± 0.01
WF4	201.6	341.5	22.77± 0.01	21.28± 0.02
WF4	90.0	535.7	22.76± 0.01	21.47± 0.02
WF4	147.4	285.9	22.98± 0.01	20.94± 0.02
WF4	223.7	108.2	22.20± 0.01	21.18± 0.02
WF4	444.4	784.5	23.10± 0.02	21.04± 0.02
WF4	284.5	159.5	23.55± 0.01	19.89± 0.01
WF4	313.5	69.6	23.44± 0.03	20.92± 0.03
WF4	661.4	86.8	23.25± 0.02	20.91± 0.02
WF4	89.7	235.4	22.54± 0.01	21.68± 0.02
WF4	75.6	145.1	23.93± 0.02	21.42± 0.02

TABLE 8. SECONDARY STANDARD STARS IN NGC 5128.— *Continued*

Chip	X (pix)	Y (pix)	V (mag)	I (mag)
WF4	384.5	215.9	22.51± 0.01	21.80± 0.02
WF4	478.5	192.3	23.41± 0.02	20.88± 0.02
WF4	574.5	170.7	22.15± 0.01	21.60± 0.02
WF4	735.1	152.9	23.53± 0.02	21.35± 0.02
WF4	719.5	73.2	23.99± 0.03	22.01± 0.03
WF4	577.4	259.0	23.01± 0.01	20.79± 0.01
WF4	419.6	327.3	23.16± 0.02	20.12± 0.01
WF4	419.2	279.9	22.21± 0.01	21.95± 0.02
WF4	446.1	275.4	22.15± 0.01	21.67± 0.02
WF4	325.4	266.8	23.65± 0.02	21.32± 0.02
WF4	375.8	254.8	22.15± 0.01	21.84± 0.02
WF4	273.9	322.2	23.36± 0.01	21.70± 0.02
WF4	250.7	387.2	23.01± 0.01	21.78± 0.02
WF4	214.1	363.5	22.98± 0.01	22.61± 0.03
WF4	130.5	300.4	23.59± 0.02	21.38± 0.02
WF4	129.5	219.9	22.71± 0.01	21.52± 0.02
WF4	170.4	466.0	22.50± 0.01	21.38± 0.02
WF4	337.9	532.2	22.88± 0.01	20.32± 0.02
WF4	297.4	476.5	23.35± 0.02	20.96± 0.02
WF4	485.8	554.7	22.94± 0.01	22.73± 0.02
WF4	556.3	752.4	22.83± 0.01	22.76± 0.03
WF4	484.5	730.3	23.70± 0.02	21.20± 0.02
WF4	130.3	709.0	23.10± 0.05	20.25± 0.02
WF4	152.4	717.3	22.01± 0.01	21.83± 0.02
WF4	96.2	752.1	22.95± 0.02	20.90± 0.02
WF4	110.6	614.0	21.70± 0.01	21.40± 0.02
WF4	151.4	572.7	22.88± 0.02	21.44± 0.02

NOTE. — X and Y position refer to the coordinate frame of the u6dm2101r observation (see Table 1).

Table 9. F555W Photometry for the NGC 5128 Cepheids.

				F555W $\pm\delta$ F555W			
JD	C1; P = 5.0d	C2; P = 5.3d	C3; P = 7.0d	C4; P = 7.3d	C5; P = 7.4d	C6; P = 8.2d	C7; P = 8.6d
2452099.00	25.38 ± 0.14	24.36 ± 0.07	24.32 ± 0.06	23.62 ± 0.04	25.07 ± 0.09	25.14 ± 0.09	23.93 ± 0.05
2452105.50	24.91 ± 0.10	24.57 ± 0.07	24.25 ± 0.06	23.99 ± 0.05	25.08 ± 0.09	25.13 ± 0.07	23.82 ± 0.04
2452112.50	25.55 ± 0.15	24.88 ± 0.08	24.31 ± 0.07	24.01 ± 0.05	25.35 ± 0.12	24.77 ± 0.05	24.38 ± 0.06
2452114.50	24.66 ± 0.08	24.42 ± 0.07	24.56 ± 0.08	23.80 ± 0.05	24.69 ± 0.09	25.43 ± 0.11	23.77 ± 0.06
2452116.75	25.17 ± 0.13	24.80 ± 0.08	23.83 ± 0.04	24.09 ± 0.05	24.90 ± 0.09	24.67 ± 0.06	23.91 ± 0.05
2452119.25	25.01 ± 0.11	24.97 ± 0.09	24.27 ± 0.06	24.21 ± 0.06	25.26 ± 0.11	24.80 ± 0.06	24.27 ± 0.06
2452123.00	25.62 ± 0.15	24.69 ± 0.10	23.69 ± 0.04	23.89 ± 0.04	24.68 ± 0.08	25.12 ± 0.08	23.78 ± 0.05
2452125.25	24.77 ± 0.08	24.27 ± 0.06	24.11 ± 0.06	24.17 ± 0.05	25.10 ± 0.11	24.51 ± 0.05	23.89 ± 0.05
2452128.75	25.32 ± 0.14	24.99 ± 0.11	24.40 ± 0.08	23.71 ± 0.05	24.97 ± 0.09	24.91 ± 0.07	24.36 ± 0.07
2452133.00	25.48 ± 0.16	24.69 ± 0.08	24.03 ± 0.05	24.20 ± 0.07	25.01 ± 0.09	24.80 ± 0.06	23.86 ± 0.04
2452137.75	25.38 ± 0.13	24.68 ± 0.08	23.84 ± 0.06	23.89 ± 0.04	24.69 ± 0.09	25.00 ± 0.08	24.53 ± 0.08
2452142.00	25.14 ± 0.11	24.43 ± 0.06	24.37 ± 0.07	24.07 ± 0.05	25.58 ± 0.15	24.56 ± 0.06	23.93 ± 0.05
				F555W $\pm\Delta$ F555W			
JD	C8; P = 8.8d	C9; P = 9.4d	C10; P = 10.6d	C11; P = 11.0d	C12; P = 11.2d	C13; P = 12.7d	C14; P = 12.7d
2452099.00	24.70 ± 0.07	23.99 ± 0.05	24.31 ± 0.07	23.88 ± 0.04	23.64 ± 0.05	25.14 ± 0.08	24.20 ± 0.08
2452105.50	25.18 ± 0.09	24.32 ± 0.07	23.77 ± 0.04	23.63 ± 0.04	23.49 ± 0.04	26.05 ± 0.18	23.55 ± 0.04
2452112.50	25.08 ± 0.09	24.12 ± 0.06	23.87 ± 0.05	24.10 ± 0.06	23.81 ± 0.05	25.29 ± 0.12	24.26 ± 0.08
2452114.50	25.21 ± 0.08	24.40 ± 0.06	24.02 ± 0.09	24.03 ± 0.05	23.95 ± 0.06	25.31 ± 0.11	24.46 ± 0.09
2452116.75	24.58 ± 0.05	24.21 ± 0.07	24.01 ± 0.05	23.67 ± 0.04	23.45 ± 0.04	25.87 ± 0.16	24.05 ± 0.06
2452119.25	24.64 ± 0.06	23.92 ± 0.06	24.27 ± 0.07	23.75 ± 0.04	23.41 ± 0.03	25.64 ± 0.12	23.48 ± 0.04
2452123.00	25.25 ± 0.10	24.21 ± 0.06	23.83 ± 0.05	24.30 ± 0.05	23.82 ± 0.05	25.03 ± 0.07	23.96 ± 0.05
2452125.25	24.82 ± 0.07	24.36 ± 0.07	23.85 ± 0.05	24.05 ± 0.04	23.96 ± 0.05	25.24 ± 0.10	24.26 ± 0.09
2452128.75	24.81 ± 0.09	-5.03 ± 0.00	24.16 ± 0.06	23.56 ± 0.03	23.30 ± 0.03	25.64 ± 0.16	24.14 ± 0.06
2452133.00	25.10 ± 0.09	24.30 ± 0.07	23.88 ± 0.05	24.13 ± 0.04	23.65 ± 0.05	25.33 ± 0.10	23.61 ± 0.04
2452137.75	24.92 ± 0.08	23.92 ± 0.05	24.02 ± 0.06	23.60 ± 0.04	23.74 ± 0.05	25.31 ± 0.10	24.15 ± 0.08
2452142.00	25.27 ± 0.11	24.23 ± 0.06	24.07 ± 0.06	23.86 ± 0.04	23.46 ± 0.04	25.65 ± 0.15	24.54 ± 0.14
				F555W $\pm\Delta$ F555W			
JD	C15; P = 12.8d	C16; P = 13.9d	C17; P = 13.9d	C18; P = 14.3d	C19; P = 14.9d	C20; P = 15.1d	C21; P = 15.1d
2452099.00	24.79 ± 0.06	23.36 ± 0.03	23.82 ± 0.06	24.44 ± 0.07	23.45 ± 0.04	23.83 ± 0.04	24.11 ± 0.08
2452105.50	24.74 ± 0.06	23.39 ± 0.04	23.57 ± 0.05	23.53 ± 0.05	23.57 ± 0.04	24.29 ± 0.06	23.51 ± 0.04
2452112.50	24.58 ± 0.06	23.41 ± 0.05	23.77 ± 0.05	24.46 ± 0.07	23.37 ± 0.04	23.68 ± 0.04	24.19 ± 0.08
2452114.50	24.25 ± 0.05	22.98 ± 0.03	23.58 ± 0.04	24.46 ± 0.09	23.61 ± 0.05	23.80 ± 0.05	23.97 ± 0.06
2452116.75	24.58 ± 0.05	23.16 ± 0.04	23.29 ± 0.04	24.20 ± 0.06	23.87 ± 0.06	24.07 ± 0.04	23.31 ± 0.04
2452119.25	24.80 ± 0.09	23.40 ± 0.04	23.56 ± 0.05	23.47 ± 0.04	23.70 ± 0.05	24.36 ± 0.06	23.38 ± 0.04
2452123.00	24.92 ± 0.06	23.60 ± 0.05	23.94 ± 0.05	24.03 ± 0.07	22.97 ± 0.04	24.02 ± 0.04	23.80 ± 0.06
2452125.25	24.68 ± 0.08	23.45 ± 0.04	24.03 ± 0.06	24.21 ± 0.07	23.23 ± 0.05	23.40 ± 0.04	24.04 ± 0.07
2452128.75	24.48 ± 0.05	22.96 ± 0.03	23.38 ± 0.04	24.57 ± 0.07	23.54 ± 0.04	23.77 ± 0.04	24.17 ± 0.07
2452133.00	24.97 ± 0.07	23.40 ± 0.05	23.52 ± 0.04	23.80 ± 0.07	23.70 ± 0.04	24.24 ± 0.04	23.21 ± 0.04
2452137.75	24.72 ± 0.07	23.67 ± 0.07	24.11 ± 0.07	24.04 ± 0.06	23.04 ± 0.04	23.99 ± 0.05	23.72 ± 0.05
2452142.00	24.49 ± 0.06	23.02 ± 0.03	23.69 ± 0.05	24.68 ± 0.12	23.45 ± 0.04	23.54 ± 0.04	24.28 ± 0.07
				F555W $\pm\Delta$ F555W			
JD	C22; P = 15.5d	C23; P = 16.1d	C24; P = 16.5d	C25; P = 16.5d	C26; P = 16.6d	C27; P = 17.3d	C28; P = 17.9d
2452099.00	23.60 ± 0.07	24.67 ± 0.06	24.20 ± 0.09	24.56 ± 0.06	23.72 ± 0.06	24.51 ± 0.05	24.06 ± 0.06
2452105.50	23.81 ± 0.04	25.13 ± 0.10	23.47 ± 0.05	25.11 ± 0.08	22.90 ± 0.04	25.37 ± 0.09	23.42 ± 0.06

Table 9. F555W Photometry for the NGC 5128 Cepheids.— *Continued*

				F555W $\pm\delta$ F555W			
2452112.50	24.00 ± 0.04	25.22 ± 0.09	24.07 ± 0.06	24.32 ± 0.05	23.60 ± 0.05	24.66 ± 0.06	23.81 ± 0.06
2452114.50	23.54 ± 0.05	24.90 ± 0.08	24.33 ± 0.06	24.53 ± 0.05	23.72 ± 0.06	24.83 ± 0.09	23.94 ± 0.05
2452116.75	23.40 ± 0.04	24.56 ± 0.07	24.25 ± 0.06	24.70 ± 0.07	23.71 ± 0.06	24.89 ± 0.10	24.03 ± 0.06
2452119.25	23.68 ± 0.05	24.93 ± 0.07	24.15 ± 0.07	25.07 ± 0.10	23.61 ± 0.05	25.16 ± 0.13	23.92 ± 0.05
2452123.00	23.98 ± 0.05	25.24 ± 0.10	23.63 ± 0.05	25.10 ± 0.09	22.95 ± 0.04	25.08 ± 0.08	23.44 ± 0.04
2452125.25	24.15 ± 0.05	25.44 ± 0.12	23.80 ± 0.04	24.90 ± 0.08	23.19 ± 0.05	24.24 ± 0.08	23.44 ± 0.05
2452128.75	23.90 ± 0.04	25.26 ± 0.10	24.08 ± 0.05	24.28 ± 0.04	23.55 ± 0.04	24.62 ± 0.08	23.77 ± 0.04
2452133.00	23.45 ± 0.03	24.65 ± 0.06	24.27 ± 0.06	24.67 ± 0.07	23.83 ± 0.07	24.67 ± 0.09	24.01 ± 0.06
2452137.75	23.92 ± 0.04	25.15 ± 0.11	23.57 ± 0.05	25.08 ± 0.10	22.98 ± 0.04	25.03 ± 0.09	23.83 ± 0.06
2452142.00	24.20 ± 0.05	25.56 ± 0.14	23.73 ± 0.04	24.79 ± 0.06	23.23 ± 0.05	24.41 ± 0.06	23.39 ± 0.04

				F555W $\pm\Delta$ F555W			
JD	C29; P = 20.5d	C30; P = 20.9d	C31; P = 21.3d	C32; P = 22.2d	C33; P = 22.4d	C34; P = 22.5d	C35; P = 22.6d
2452099.00	24.18 ± 0.05	24.36 ± 0.05	23.99 ± 0.04	23.73 ± 0.07	23.87 ± 0.06	24.34 ± 0.06	25.28 ± 0.11
2452105.50	23.89 ± 0.05	24.69 ± 0.06	22.99 ± 0.03	24.11 ± 0.05	23.01 ± 0.04	24.76 ± 0.08	-5.06 ± 0.00
2452112.50	23.65 ± 0.04	23.80 ± 0.04	23.55 ± 0.03	24.66 ± 0.07	23.43 ± 0.05	24.89 ± 0.09	24.65 ± 0.07
2452114.50	23.81 ± 0.05	23.97 ± 0.04	23.73 ± 0.04	24.60 ± 0.08	23.59 ± 0.06	24.72 ± 0.08	24.76 ± 0.08
2452116.75	24.06 ± 0.05	24.07 ± 0.06	23.89 ± 0.04	24.44 ± 0.06	23.76 ± 0.05	24.80 ± 0.08	24.72 ± 0.08
2452119.25	24.23 ± 0.05	24.20 ± 0.05	23.99 ± 0.04	23.49 ± 0.04	23.75 ± 0.04	24.26 ± 0.05	24.89 ± 0.07
2452123.00	24.36 ± 0.06	24.53 ± 0.05	23.86 ± 0.04	23.73 ± 0.04	23.95 ± 0.05	24.44 ± 0.06	25.45 ± 0.10
2452125.25	24.27 ± 0.06	24.71 ± 0.07	23.26 ± 0.03	23.92 ± 0.05	23.73 ± 0.04	24.46 ± 0.09	25.43 ± 0.12
2452128.75	23.34 ± 0.03	24.61 ± 0.07	23.16 ± 0.03	24.37 ± 0.09	22.49 ± 0.03	24.79 ± 0.07	25.20 ± 0.09
2452133.00	23.65 ± 0.04	23.75 ± 0.04	23.48 ± 0.03	24.46 ± 0.06	23.02 ± 0.06	25.00 ± 0.09	24.25 ± 0.06
2452137.75	24.22 ± 0.17	24.09 ± 0.05	23.82 ± 0.04	24.61 ± 0.07	23.50 ± 0.04	24.77 ± 0.09	24.88 ± 0.08
2452142.00	24.22 ± 0.05	24.41 ± 0.06	23.99 ± 0.04	23.55 ± 0.04	23.74 ± 0.05	24.18 ± 0.05	25.12 ± 0.08

				F555W $\pm\Delta$ F555W			
JD	C36; P = 23.1d	C37; P = 23.1d	C38; P = 24.1d	C39; P = 26.4d	C40; P = 27.1d	C41; P = 27.8d	C42; P = 30.5d
2452099.00	22.97 ± 0.03	22.66 ± 0.04	23.32 ± 0.03	22.96 ± 0.03	23.39 ± 0.05	24.23 ± 0.05	22.87 ± 0.04
2452105.50	22.86 ± 0.03	23.19 ± 0.06	23.75 ± 0.04	23.32 ± 0.03	23.04 ± 0.03	23.06 ± 0.03	23.13 ± 0.04
2452112.50	23.19 ± 0.03	23.61 ± 0.07	23.70 ± 0.03	23.80 ± 0.04	23.40 ± 0.03	23.64 ± 0.05	23.48 ± 0.04
2452114.50	23.35 ± 0.04	23.56 ± 0.06	22.86 ± 0.04	23.72 ± 0.04	23.57 ± 0.04	23.69 ± 0.04	23.61 ± 0.04
2452116.75	23.33 ± 0.03	23.45 ± 0.07	22.86 ± 0.03	23.68 ± 0.04	23.59 ± 0.04	23.82 ± 0.05	23.74 ± 0.05
2452119.25	23.25 ± 0.04	22.53 ± 0.05	23.03 ± 0.03	23.33 ± 0.03	23.61 ± 0.04	23.91 ± 0.05	23.83 ± 0.05
2452123.00	22.75 ± 0.03	22.59 ± 0.04	23.28 ± 0.03	22.85 ± 0.03	23.69 ± 0.03	24.16 ± 0.06	23.52 ± 0.08
2452125.25	22.67 ± 0.03	22.90 ± 0.05	23.50 ± 0.03	22.95 ± 0.03	23.58 ± 0.04	24.19 ± 0.06	23.78 ± 0.05
2452128.75	22.77 ± 0.03	23.09 ± 0.19	23.72 ± 0.03	23.16 ± 0.03	22.98 ± 0.03	24.19 ± 0.05	23.06 ± 0.04
2452133.00	22.89 ± 0.05	23.45 ± 0.06	23.81 ± 0.04	23.43 ± 0.03	23.13 ± 0.03	23.06 ± 0.03	23.00 ± 0.04
2452137.75	23.31 ± 0.04	23.20 ± 0.22	23.30 ± 0.03	23.72 ± 0.05	23.33 ± 0.03	23.43 ± 0.03	23.32 ± 0.05
2452142.00	23.39 ± 0.04	22.55 ± 0.04	22.94 ± 0.03	23.74 ± 0.04	23.44 ± 0.03	23.69 ± 0.04	23.45 ± 0.05

				F555W $\pm\Delta$ F555W			
JD	C43; P = 34.1d	C44; P = 34.7d	C45; P = 41.2d	C46; P = 42.8d	C47; P = 44.0d	C48; P = 44.0d	C49; P = 44.4d
2452099.00	24.85 ± 0.08	24.68 ± 0.08	23.27 ± 0.03	24.22 ± 0.09	23.04 ± 0.03	23.95 ± 0.06	23.22 ± 0.04
2452105.50	24.47 ± 0.08	24.01 ± 0.05	23.50 ± 0.04	24.40 ± 0.07	23.11 ± 0.04	24.13 ± 0.06	23.45 ± 0.03
2452112.50	24.49 ± 0.07	24.00 ± 0.04	23.83 ± 0.04	24.64 ± 0.08	23.28 ± 0.03	24.28 ± 0.06	23.60 ± 0.05
2452114.50	24.68 ± 0.08	24.10 ± 0.05	23.85 ± 0.04	24.73 ± 0.08	23.29 ± 0.03	24.26 ± 0.06	23.53 ± 0.04
2452116.75	24.67 ± 0.07	24.14 ± 0.08	23.96 ± 0.04	24.57 ± 0.11	23.29 ± 0.04	24.34 ± 0.08	23.50 ± 0.05
2452119.25	24.82 ± 0.08	24.27 ± 0.05	24.09 ± 0.05	24.79 ± 0.10	23.30 ± 0.04	24.35 ± 0.08	23.23 ± 0.04

Table 9. F555W Photometry for the NGC 5128 Cepheids.— *Continued*

				F555W $\pm\delta$ F555W			
2452123.00	25.11 ± 0.10	24.37 ± 0.06	24.19 ± 0.05	24.77 ± 0.09	23.40 ± 0.03	24.54 ± 0.07	22.81 ± 0.03
2452125.25	25.39 ± 0.12	24.48 ± 0.06	24.04 ± 0.06	24.58 ± 0.08	23.43 ± 0.03	24.37 ± 0.09	22.83 ± 0.04
2452128.75	25.44 ± 0.10	24.56 ± 0.06	24.31 ± 0.06	24.16 ± 0.06	23.53 ± 0.03	24.59 ± 0.10	22.75 ± 0.03
2452133.00	24.98 ± 0.09	24.74 ± 0.06	23.75 ± 0.04	24.00 ± 0.05	23.56 ± 0.04	24.78 ± 0.14	22.85 ± 0.03
2452137.75	24.53 ± 0.07	24.26 ± 0.05	23.29 ± 0.04	24.15 ± 0.07	23.63 ± 0.06	24.85 ± 0.09	23.08 ± 0.03
2452142.00	24.53 ± 0.09	23.75 ± 0.04	23.38 ± 0.04	24.23 ± 0.06	23.69 ± 0.04	25.00 ± 0.11	23.17 ± 0.03
				F555W $\pm\Delta$ F555W			
JD	C50; P = 47.0d	C51; P = 48.0d	C52; P = 48.5d	C53; P = 48.5d	C54; P = 50.4d	C55; P = 74.0d	C56; P = 80.0d
2452099.00	24.20 ± 0.06	24.91 ± 0.09	24.43 ± 0.06	22.36 ± 0.03	23.44 ± 0.04	25.42 ± 0.15	24.50 ± 0.08
2452105.50	23.76 ± 0.05	24.75 ± 0.07	24.53 ± 0.06	22.83 ± 0.03	23.50 ± 0.04	25.49 ± 0.15	24.55 ± 0.07
2452112.50	24.18 ± 0.05	24.83 ± 0.08	24.68 ± 0.09	22.76 ± 0.04	23.72 ± 0.05	25.34 ± 0.13	24.31 ± 0.07
2452114.50	24.22 ± 0.05	24.84 ± 0.08	24.89 ± 0.08	22.51 ± 0.04	23.62 ± 0.04	25.39 ± 0.13	24.23 ± 0.07
2452116.75	24.33 ± 0.06	24.98 ± 0.10	25.05 ± 0.08	22.00 ± 0.03	23.66 ± 0.04	25.07 ± 0.10	24.28 ± 0.06
2452119.25	24.35 ± 0.05	24.92 ± 0.10	25.31 ± 0.10	21.94 ± 0.03	23.72 ± 0.04	25.13 ± 0.11	24.23 ± 0.06
2452123.00	24.38 ± 0.06	25.16 ± 0.11	25.52 ± 0.12	22.03 ± 0.03	23.68 ± 0.05	24.73 ± 0.10	24.06 ± 0.06
2452125.25	24.48 ± 0.06	25.10 ± 0.10	25.75 ± 0.16	22.04 ± 0.02	23.79 ± 0.04	24.81 ± 0.09	24.08 ± 0.05
2452128.75	24.51 ± 0.06	25.21 ± 0.10	25.77 ± 0.15	22.19 ± 0.03	23.69 ± 0.05	24.61 ± 0.07	23.87 ± 0.05
2452133.00	24.69 ± 0.07	25.50 ± 0.13	25.94 ± 0.15	22.27 ± 0.03	23.67 ± 0.05	24.57 ± 0.07	23.84 ± 0.05
2452137.75	24.58 ± 0.06	25.51 ± 0.13	25.67 ± 0.13	22.40 ± 0.02	23.56 ± 0.05	24.70 ± 0.09	23.95 ± 0.05
2452142.00	24.66 ± 0.08	25.65 ± 0.15	24.74 ± 0.09	22.55 ± 0.04	23.31 ± 0.08	24.70 ± 0.09	23.84 ± 0.04

Table 10. F814W Photometry for the NGC 5128 Cepheids.

F814W $\pm\delta$ F814W							
JD	C1; P = 5.0d	C2; P = 5.3d	C3; P = 7.0d	C4; P = 7.3d	C5; P = 7.4d	C6; P = 8.2d	C7; P = 8.6d
2452099.00	24.20 ± 0.11	23.42 ± 0.07	23.59 ± 0.08	23.06 ± 0.05	24.09 ± 0.12	23.95 ± 0.08	23.00 ± 0.06
2452112.75	24.17 ± 0.12	23.51 ± 0.08	23.66 ± 0.09	23.29 ± 0.06	24.04 ± 0.13	23.60 ± 0.07	23.26 ± 0.08
2452117.00	24.09 ± 0.13	23.48 ± 0.07	23.36 ± 0.06	23.33 ± 0.07	23.89 ± 0.11	23.64 ± 0.06	23.08 ± 0.06
2452123.25	24.43 ± 0.16	23.61 ± 0.08	23.17 ± 0.10	23.15 ± 0.05	23.83 ± 0.10	23.84 ± 0.08	22.39 ± 0.09
2452129.00	24.58 ± 0.17	23.87 ± 0.09	23.60 ± 0.06	23.10 ± 0.06	24.25 ± 0.27	23.64 ± 0.07	23.42 ± 0.05
2452137.75	24.28 ± 0.14	23.47 ± 0.08	23.32 ± 0.06	23.13 ± 0.06	23.82 ± 0.11	23.76 ± 0.07	23.48 ± 0.09
F814W $\pm\Delta$ F814W							
JD	C8; P = 8.8d	C9; P = 9.4d	C10; P = 10.6d	C11; P = 11.0d	C12; P = 11.2d	C13; P = 12.7d	C14; P = 12.7d
2452099.00	23.36 ± 0.07	22.80 ± 0.06	23.33 ± 0.09	22.92 ± 0.01	22.74 ± 0.01	23.40 ± 0.06	22.98 ± 0.01
2452112.75	23.46 ± 0.06	23.03 ± 0.06	22.84 ± 0.08	23.33 ± 0.06	22.76 ± 0.07	23.55 ± 0.08	23.12 ± 0.07
2452117.00	23.27 ± 0.08	22.99 ± 0.08	22.97 ± 0.06	22.94 ± 0.01	22.71 ± 0.01	23.93 ± 0.10	23.13 ± 0.01
2452123.25	23.55 ± 0.09	23.00 ± 0.01	22.94 ± 0.05	23.31 ± 0.06	22.82 ± 0.01	23.34 ± 0.07	22.99 ± 0.06
2452129.00	23.37 ± 0.07	-4.89 ± 0.01	23.21 ± 0.06	22.80 ± 0.01	22.56 ± 0.01	23.73 ± 0.07	22.94 ± 0.01
2452137.75	23.34 ± 0.07	22.92 ± 0.01	22.87 ± 0.07	23.00 ± 0.01	22.88 ± 0.07	23.41 ± 0.06	23.08 ± 0.07
F814W $\pm\Delta$ F814W							
JD	C15; P = 12.8d	C16; P = 13.9d	C17; P = 13.9d	C18; P = 14.3d	C19; P = 14.9d	C20; P = 15.1d	C21; P = 15.1d
2452099.00	23.44 ± 0.08	22.52 ± 0.01	22.72 ± 0.01	23.15 ± 0.01	22.48 ± 0.01	22.75 ± 0.01	23.07 ± 0.10
2452112.75	23.23 ± 0.01	22.38 ± 0.01	22.73 ± 0.01	23.11 ± 0.06	22.47 ± 0.01	22.66 ± 0.01	23.11 ± 0.09
2452117.00	23.13 ± 0.06	22.37 ± 0.01	22.51 ± 0.01	23.03 ± 0.01	22.84 ± 0.01	23.02 ± 0.01	22.60 ± 0.06
2452123.25	23.45 ± 0.06	22.57 ± 0.06	22.62 ± 0.01	22.83 ± 0.01	22.25 ± 0.01	23.02 ± 0.01	22.94 ± 0.08
2452129.00	23.11 ± 0.01	22.26 ± 0.01	22.48 ± 0.01	23.23 ± 0.07	22.02 ± 0.09	22.65 ± 0.01	22.92 ± 0.06
2452137.75	23.33 ± 0.07	22.71 ± 0.01	22.97 ± 0.06	22.82 ± 0.01	22.27 ± 0.01	23.03 ± 0.01	22.79 ± 0.08
F814W $\pm\Delta$ F814W							
JD	C22; P = 15.5d	C23; P = 16.1d	C24; P = 16.5d	C25; P = 16.5d	C26; P = 16.6d	C27; P = 17.3d	C28; P = 17.9d
2452099.00	22.61 ± 0.01	23.06 ± 0.06	23.16 ± 0.07	22.91 ± 0.01	22.61 ± 0.08	23.21 ± 0.01	22.88 ± 0.07
2452112.75	22.80 ± 0.01	23.23 ± 0.07	22.91 ± 0.06	22.78 ± 0.01	22.44 ± 0.08	23.17 ± 0.01	22.65 ± 0.01
2452117.00	22.22 ± 0.01	22.94 ± 0.01	23.07 ± 0.07	22.90 ± 0.01	22.77 ± 0.18	23.29 ± 0.06	22.85 ± 0.07
2452123.25	22.75 ± 0.01	23.29 ± 0.07	22.59 ± 0.01	23.21 ± 0.01	22.08 ± 0.01	23.56 ± 0.06	22.45 ± 0.01
2452129.00	22.81 ± 0.01	23.35 ± 0.06	22.96 ± 0.06	22.81 ± 0.01	22.48 ± 0.01	23.12 ± 0.01	22.65 ± 0.01
2452137.75	22.70 ± 0.01	23.19 ± 0.01	22.57 ± 0.01	23.24 ± 0.01	22.19 ± 0.06	23.55 ± 0.06	22.83 ± 0.06
F814W $\pm\Delta$ F814W							
JD	C29; P = 20.5d	C30; P = 20.9d	C31; P = 21.3d	C32; P = 22.2d	C33; P = 22.4d	C34; P = 22.5d	C35; P = 22.6d
2452099.00	22.53 ± 0.09	22.90 ± 0.01	22.79 ± 0.01	22.47 ± 0.01	22.68 ± 0.01	22.72 ± 0.06	23.12 ± 0.01
2452112.75	22.38 ± 0.01	22.63 ± 0.01	22.40 ± 0.01	22.98 ± 0.01	22.12 ± 0.01	23.10 ± 0.06	22.77 ± 0.01
2452117.00	22.49 ± 0.01	22.75 ± 0.01	22.42 ± 0.06	22.93 ± 0.01	22.41 ± 0.01	22.97 ± 0.05	22.89 ± 0.07
2452123.25	22.88 ± 0.07	23.00 ± 0.01	22.78 ± 0.01	22.45 ± 0.01	22.59 ± 0.01	22.83 ± 0.05	23.16 ± 0.06
2452129.00	22.21 ± 0.01	23.14 ± 0.06	22.24 ± 0.01	22.70 ± 0.01	21.93 ± 0.01	23.09 ± 0.06	23.23 ± 0.07
2452137.75	22.47 ± 0.08	22.74 ± 0.01	22.65 ± 0.01	22.99 ± 0.01	22.24 ± 0.01	22.97 ± 0.05	22.73 ± 0.06
F814W $\pm\Delta$ F814W							

Table 10. F814W Photometry for the NGC 5128 Cepheids.— *Continued*

F814W $\pm\delta$ F814W							
JD	C36; P = 23.1d	C37; P = 23.1d	C38; P = 24.1d	C39; P = 26.4d	C40; P = 27.1d	C41; P = 27.8d	C42; P = 30.5d
2452099.00	22.13 ± 0.01	21.40 ± 0.07	22.19 ± 0.01	22.01 ± 0.01	22.28 ± 0.07	22.78 ± 0.01	21.90 ± 0.01
2452112.75	22.20 ± 0.01	22.27 ± 0.07	22.61 ± 0.01	22.49 ± 0.01	22.33 ± 0.01	22.35 ± 0.01	22.16 ± 0.01
2452117.00	22.42 ± 0.01	22.18 ± 0.07	21.99 ± 0.01	22.55 ± 0.01	22.44 ± 0.01	22.36 ± 0.01	22.41 ± 0.01
2452123.25	21.92 ± 0.01	21.71 ± 0.01	22.19 ± 0.01	21.98 ± 0.01	22.60 ± 0.01	22.59 ± 0.01	22.52 ± 0.01
2452129.00	21.98 ± 0.01	21.61 ± 0.08	22.52 ± 0.01	22.09 ± 0.01	22.09 ± 0.01	22.78 ± 0.01	22.01 ± 0.01
2452137.75	22.26 ± 0.01	22.15 ± 0.10	22.33 ± 0.01	22.49 ± 0.01	22.27 ± 0.01	22.13 ± 0.01	22.06 ± 0.01
F814W $\pm\Delta$ F814W							
JD	C43; P = 34.1d	C44; P = 34.7d	C45; P = 41.2d	C46; P = 42.8d	C47; P = 44.0d	C48; P = 44.0d	C49; P = 44.4d
2452099.00	24.02 ± 0.11	22.60 ± 0.01	21.72 ± 0.01	22.24 ± 0.01	21.51 ± 0.05	22.31 ± 0.05	21.69 ± 0.05
2452112.75	23.88 ± 0.12	22.15 ± 0.01	21.86 ± 0.01	22.51 ± 0.01	21.49 ± 0.05	22.38 ± 0.05	22.06 ± 0.05
2452117.00	24.07 ± 0.12	22.20 ± 0.01	22.06 ± 0.01	22.55 ± 0.01	21.62 ± 0.05	22.41 ± 0.05	22.03 ± 0.05
2452123.25	24.43 ± 0.23	22.34 ± 0.01	22.20 ± 0.01	22.57 ± 0.01	21.63 ± 0.05	22.45 ± 0.05	21.58 ± 0.05
2452129.00	24.34 ± 0.15	22.52 ± 0.01	22.31 ± 0.01	22.18 ± 0.01	21.75 ± 0.05	22.50 ± 0.05	21.53 ± 0.05
2452137.75	23.78 ± 0.11	22.14 ± 0.01	21.73 ± 0.01	22.15 ± 0.01	21.77 ± 0.05	22.59 ± 0.05	21.63 ± 0.05
F814W $\pm\Delta$ F814W							
JD	C50; P = 47.0d	C51; P = 48.0d	C52; P = 48.5d	C53; P = 48.5d	C54; P = 50.4d	C55; P = 74.0d	C56; P = 80.0d
2452099.00	23.19 ± 0.06	22.91 ± 0.05	23.74 ± 0.08	21.50 ± 0.01	22.57 ± 0.05	22.93 ± 0.06	23.19 ± 0.06
2452112.75	23.17 ± 0.05	22.80 ± 0.05	23.87 ± 0.08	21.65 ± 0.01	22.81 ± 0.08	22.90 ± 0.06	23.20 ± 0.07
2452117.00	23.29 ± 0.06	22.87 ± 0.05	23.86 ± 0.09	21.27 ± 0.01	22.69 ± 0.06	22.94 ± 0.05	23.05 ± 0.05
2452123.25	23.47 ± 0.06	22.96 ± 0.05	24.35 ± 0.12	21.22 ± 0.01	22.78 ± 0.06	22.76 ± 0.06	22.83 ± 0.05
2452129.00	23.61 ± 0.08	23.03 ± 0.05	24.46 ± 0.14	21.24 ± 0.01	22.88 ± 0.05	22.50 ± 0.07	22.66 ± 0.06
2452137.75	23.60 ± 0.09	23.14 ± 0.05	24.55 ± 0.15	21.37 ± 0.01	22.78 ± 0.05	22.66 ± 0.05	22.78 ± 0.05

Table 11. Suspected Variable Stars in NGC 5128.

ID	X (pixel)	Y (pixel)	RA (h:m:s)	Dec (°:′:″)	Period (days)	V^{Int} (mag)	I^{Int} (mag)	V^{ph} (mag)	I^{ph} (mag)	Chip
V1	477.0	384.2	13:25:17.853	−43:00:11.30	5.2	25.76	24.45	25.80	24.37	PC
V2	244.4	592.1	13:25:20.198	−42:59:29.75	5.3	23.62	22.76	23.63	22.76	WF4
V3	633.1	95.7	13:25:15.042	−42:59:03.10	5.6	24.40	23.14	24.41	23.14	WF4
V4	241.4	647.5	13:25:12.689	−42:59:07.93	5.8	24.32	23.55	24.30	23.59	WF3
V5	383.6	563.3	13:25:19.665	−42:59:16.90	6.2	24.39	22.95	24.34	22.94	WF4
V6	387.4	314.7	13:25:17.458	−42:59:22.04	6.3	24.26	23.05	24.19	23.03	WF4
V7	433.1	411.9	13:25:18.227	−42:59:15.45	6.3	24.17	23.23	24.20	23.25	WF4
V8	124.3	112.0	13:25:15.183	−43:00:10.38	6.4	24.39	23.09	24.40	23.12	WF2
V9	274.2	709.5	13:25:21.170	−42:59:24.26	6.7	24.29	23.88	24.24	23.92	WF4
V10	636.8	342.9	13:25:18.457	−43:00:07.82	6.8	25.36	24.02	25.45	24.07	PC
V11	423.9	632.9	13:25:11.113	−42:59:13.50	6.8	24.20	23.30	24.22	23.33	WF3
V12	532.8	218.3	13:25:16.316	−42:59:10.07	6.8	24.64	23.64	24.63	23.67	WF4
V13	522.7	269.0	13:25:17.928	−43:00:05.74	6.9	25.14	23.97	25.16	23.96	PC
V14	336.4	481.9	13:25:19.041	−42:59:23.29	7.0	23.77	22.98	23.83	23.01	WF4
V15	195.8	383.2	13:25:13.647	−42:59:32.38	7.2	24.51	22.16	24.52	22.16	WF3
V16	416.2	204.5	13:25:16.427	−42:59:21.67	7.2	23.82	23.60	23.82	23.57	WF4
V17	454.9	262.4	13:25:16.861	−42:59:16.64	7.2	24.34	23.15	24.32	23.11	WF4
V18	357.2	426.7	13:25:18.510	−42:59:22.49	7.3	24.06	23.06	24.10	23.11	WF4
V19	334.9	506.7	13:25:19.263	−42:59:22.88	7.3	24.05	23.02	24.09	23.03	WF4
V20	602.2	549.3	13:25:09.717	−42:59:25.67	7.4	24.73	23.59	24.79	23.62	WF3
V21	410.0	120.6	13:25:15.724	−43:00:38.06	7.4	24.30	23.11	24.27	23.09	WF2
V22	596.0	93.0	13:25:15.091	−42:59:06.74	7.5	24.28	23.50	24.32	23.54	WF4
V23	593.0	142.6	13:25:15.531	−42:59:05.93	7.6	24.26	23.45	24.21	23.38	WF4
V24	376.3	575.6	13:25:19.788	−42:59:17.34	7.9	24.10	23.13	24.10	23.12	WF4
V25	313.9	658.5	13:25:20.643	−42:59:21.56	8.2	23.94	22.94	23.88	22.91	WF4
V26	476.6	518.7	13:25:19.084	−42:59:08.88	8.4	24.20	23.38	24.19	23.34	WF4
V27	704.7	663.6	13:25:08.586	−42:59:17.05	8.5	24.53	23.45	24.51	23.44	WF3
V28	158.1	643.4	13:25:13.429	−42:59:06.44	8.8	23.76	23.12	23.70	23.10	WF3
V29	314.6	344.2	13:25:17.866	−42:59:28.45	8.8	24.62	23.52	24.65	23.52	WF4
V30	372.6	406.1	13:25:18.297	−42:59:21.45	9.1	24.18	23.81	24.23	23.84	WF4
V31	356.3	414.3	13:25:18.402	−42:59:22.85	9.4	24.32	22.99	24.28	22.96	WF4
V32	272.7	548.1	13:25:12.623	−42:59:18.20	9.5	23.96	23.05	23.95	23.05	WF3
V33	118.6	613.0	13:25:13.840	−42:59:08.47	9.7	24.58	23.81	24.56	23.79	WF3
V34	465.6	310.4	13:25:11.421	−42:59:45.62	9.8	25.74	23.74	25.72	23.72	WF3
V35	207.9	381.6	13:25:12.993	−43:00:24.68	10.4	25.08	23.30	25.08	23.31	WF2
V36	271.3	133.8	13:25:16.786	−43:00:02.39	10.7	25.01	23.74	25.04	23.75	PC
V37	376.1	310.5	13:25:17.443	−42:59:23.22	11.6	24.07	23.17	24.03	23.14	WF4
V38	92.3	630.8	13:25:14.031	−42:59:06.17	11.7	23.83	22.67	23.82	22.66	WF3
V39	338.2	435.0	13:25:18.622	−42:59:24.15	12.7	23.77	22.97	23.74	22.96	WF4
V40	418.1	379.9	13:25:17.973	−42:59:17.61	13.7	23.79	22.76	23.84	22.82	WF4
V41	99.8	445.4	13:25:14.359	−42:59:24.17	13.9	24.81	23.01	24.87	22.94	WF3
V42	333.2	141.0	13:25:12.941	−42:59:58.92	14.6	25.33	23.24	25.37	23.25	WF3
V43	324.8	515.3	13:25:19.359	−42:59:23.67	15.6	23.69	22.58	23.69	22.59	WF4
V44	246.3	556.4	13:25:19.880	−42:59:30.36	15.6	23.56	22.60	23.52	22.58	WF4
V45	540.4	578.9	13:25:18.292	−43:00:19.25	17.8	25.71	23.31	25.67	23.28	PC
V46	249.3	556.0	13:25:19.870	−42:59:30.08	19.5	23.83	22.83	23.81	22.78	WF4
V47	670.1	482.2	13:25:18.722	−43:00:13.63	20.4	25.15	23.28	25.22	23.33	PC
V48	190.6	579.7	13:25:20.195	−42:59:35.23	20.8	23.56	22.51	23.44	22.47	WF4
V49	197.6	741.9	13:25:09.809	−43:00:32.22	28.0	25.16	23.76	25.17	23.77	WF2
V50	140.8	339.5	13:25:16.455	−43:00:12.82	29.2	25.06	24.13	25.07	24.14	PC
V51	69.0	679.1	13:25:14.131	−42:59:01.04	29.2	23.04	21.93	23.03	21.92	WF3
V52	767.8	495.4	13:25:13.191	−43:01:21.27	29.7	24.64	23.58	24.65	23.58	WF2
V53	156.2	309.5	13:25:17.878	−42:59:44.53	≥30.0	25.22	22.79	25.27	22.82	WF4
V54	718.2	688.8	13:25:08.418	−42:59:14.95	≥32.0	25.34	24.15	25.34	24.14	WF3
V55	595.9	474.0	13:25:13.011	−43:01:04.31	≥44.0	25.48	23.66	25.47	23.67	WF2
V56	599.0	714.2	13:25:09.407	−42:59:09.75	≥44.0	24.64	23.61	24.64	23.63	WF3
V57	340.2	701.6	13:25:10.462	−43:00:44.99	≥45.0	24.28	22.19	24.28	22.19	WF2
V58	110.5	677.8	13:25:13.773	−42:59:02.08	≥45.0	24.25	22.85	24.27	22.87	WF3
V59	360.5	749.0	13:25:21.343	−42:59:15.04	≥45.0	25.08	23.62	25.09	23.58	WF4
V60	289.6	576.4	13:25:12.415	−42:59:15.86	≥48.0	23.66	23.17	23.66	23.16	WF3
V61	522.7	691.8	13:25:10.940	−43:01:02.33	≥49.6	24.17	23.10	24.18	23.11	WF2
V62	387.0	319.3	13:25:12.095	−42:59:42.95	49.6	25.13	22.88	25.11	22.88	WF3
V63	550.7	215.7	13:25:16.258	−42:59:08.39	≥50.0	24.36	22.54	24.38	22.55	WF4
V64	581.4	696.8	13:25:11.023	−43:01:08.09	≥55.0	25.73	23.49	25.68	23.46	WF2
V65	327.7	198.9	13:25:12.870	−42:59:53.21	≥60.0	25.75	23.14	25.86	23.17	WF3
V66	300.0	402.2	13:25:12.689	−42:59:32.93	≥70.0	26.03	23.02	26.08	23.07	WF3
V67	294.2	145.8	13:25:15.254	−43:00:27.48	≥80.0	23.23	23.30	23.14	23.28	WF2
V68	166.1	276.3	13:25:14.131	−42:59:42.02	≥80.0	25.59	23.15	25.48	23.10	WF3
V69	297.6	589.2	13:25:20.066	−42:59:24.67	≥80.0	23.39	23.02	23.29	22.99	WF4
V70	345.3	176.8	13:25:16.326	−42:59:29.15	≥80.0	24.36	22.11	24.35	22.13	WF4

TABLE 11. SUSPECTED VARIABLE STARS IN NGC 5128.— *Continued*

ID	X (pixel)	Y (pixel)	RA (h:m:s)	Dec (°:′:″)	Period (days)	V^{Int} (mag)	I^{Int} (mag)	V^{ph} (mag)	I^{ph} (mag)	Chip

NOTE. — Comments on the individual Variables: V1: found in region of high background and likely contaminated; the light curve is noisy. V2: located five pixels from a very bright star; the resulting bias in the photometry might be responsible for the low amplitude of the light curve. V3: found in a crowded region. V4: it appears to be a blend from visual inspection. V5, V6, V7: all found in a crowded region. V8: it appears to be a blend based on visual inspection, possibly resulting in a light curve with low amplitude. V9: found in a crowded region; the resulting bias in the photometry might be responsible for the low amplitude of the light curve. V10 and V11: the light variations are not entirely convincing from a visual inspection, the light curve has small amplitude. V12: found in a crowded region. V13: located two pixels away from a bright star. V14: found in a crowded region. V15: the light variations are not entirely convincing from a visual inspection. V16: found in a crowded region; the resulting bias in the photometry might be responsible for the low amplitude of the light curve. V17 to V21: found in a crowded region; the light curve of V20 is symmetric. V22: located close to the diffraction spike of a bright star; the light curve is noisy. V23: it appears to be a blend on visual inspection. V24: located ten pixels away from a bright star; the resulting bias in the photometry might be responsible for the symmetric nature of the light curve. V25: found in a crowded region. V26: the light variations are not entirely convincing from a visual inspection. V27: the light curve appears to be rather symmetric. V28 to V34: found in a crowded region; the light curves are symmetric and/or noisy. V35: the light curve appears to be rather symmetric. V36 and V37: found in crowded region; the light curve of V36 is noisy. V38: it appears to be a blend on visual inspection. V39 to V44: found in crowded region; the light curves are noisy and/or symmetric. V45: the light curve is noisy. V46: found in crowded region. V47: it appears to be a blend on visual inspection. V48 and V49: found in crowded region; the light curves are noisy. V50: the light curve is noisy. V51: it appears to be a blend on visual inspection. V52: found very close to the edge of the chip; the photometry might be contaminated, possibly resulting in the flat minimum of the light curve. V53 to V56: found in crowded region; some light curves are noisy or symmetric. V57: the light variations are not entirely convincing from a visual inspection. V58: found in crowded region; the light curve has small amplitude. V59: the light variations are not entirely convincing from a visual inspection. V60: found in crowded region; the light curve has small amplitude. V61: located four pixels away from a bright star; the photometry might be contaminated, possibly resulting in the small amplitude observed for the light curve. V62: it appears to be a blend on visual inspection. V63: found in a crowded region, the light curve has slow ascent. V64 and V65: the light variations are not entirely convincing from a visual inspection. V66: found in a crowded region. V67: the light curve has very sparse phase coverage, the nature of the variations could not be established. V68 to V70: found in crowded region.

NOTE: Figures 11 to 13 can be found on the version of the paper available at http://astrowww.phys.uvic.ca∼lff/publications.html